Spin-related phenomena in the two-dimensional hopping regime in magnetic field

A. V. Shumilin, D. S. Smirnov, and L. E. Golub
Ioffe Institute, 194021 St. Petersburg, Russia

(Received 14 May 2018; revised manuscript received 23 August 2018; published 5 October 2018)

The spin relaxation time of localized charge carriers is a few orders of magnitude larger than that of free electrons and holes. Therefore, mutual conversion of spin polarization, charge current, and spin current turns out to be underlined in the hopping conductivity regime. We reveal different regimes of the coupled spin and charge dynamics depending on the relation between the spin relaxation time and the characteristic hopping time. We derive kinetic equations to describe electrical spin orientation, dc spin Hall effect, and spin-galvanic effect in the transverse magnetic field. The generalized macroscopic conductivities describing these effects are calculated using percolation theory supported by numerical simulation. The conductivities change the sign at least once as functions of magnetic field for all values of the spin relaxation time.

DOI: 10.1103/PhysRevB.98.155304

I. INTRODUCTION

Spin is in the center of condensed-matter physics for almost two decades due to remarkable effects allowing for both deeper understanding of fundamental physical processes and some possible future applications [1]. One of the most investigated spin-related phenomena is the spin Hall effect (SHE) which is a conversion of an electric current into spin current [2–5]. There is also an inverse effect (inverse SHE) consisting in the generation of the electric current under the spin current flow [2,6–8]. The SHE is qualitatively similar to the ordinary Hall effect: the electric current in the system is converted into the spin current or spin-up and spin-down separation in the perpendicular direction. This means that the charge carriers with opposite spins flow preferentially in opposite directions. Microscopically, SHE arises due to spin-orbit interaction, and it is symmetry allowed in any system. There are some more subtle spin-dependent phenomena which take place only in systems of low point symmetry. The first example is the current-induced spin orientation (CISP) consisting in the generation of a net spin polarization by electric current [9–15]. The reciprocal phenomenon, the spin galvanic effect (SGE), is a generation of electrical current in the process of nonequilibrium spin relaxation [16]. Both CISP and SGE are symmetry allowed in gyrotropic (optically active) systems. They have been investigated in gyrotropic bulk semiconductors, for example, tellurium [9,10], strained zinc-blende III-V crystals, and in various two-dimensional (2D) heterostructures [17–20]. CISP and SGE can be viewed as the consequences of SHE (or inverse SHE), so all three spin-related phenomena are interconnected [21]. The microscopic source for the conversion of the spin current into the net spin polarization (CISP) and to electric current (SGE) is the spin-momentum linear coupling caused by Rashba- and 2D Dresselhaus spin-orbit interactions [22–25].

Aside from the spin-dependent effects related with the electric current flow, there is a rich spin physics of carriers localized at neutral dopants, interfaces of semiconductor heterostructures, and in quantum dots. These systems attract permanent interest due to long spin relaxation times which can be by orders of magnitude larger than for free carriers and vary in a broad range [26]. The reason for long spin lifetimes is that the major mechanisms of spin relaxation related with free carrier momentum scattering are absent for localized carriers, and spin relaxation is determined by a weak hyperfine interaction with host lattice nuclei [27,28]. Long spin memory allows for fast spin manipulation by optical pulses [29–31], resonant spin amplification [32,33], electron spin precession mode locking [34–38], nuclei-induced frequency focusing [39–43], and measurement of spin fluctuations [44–47].

The two groups of the above-described spin-dependent effects, related with the electrical current flow and with the long-lived localized spins, meet in systems with hopping conductivity. Indeed, if the localized carriers can migrate between the localization sites, then one can study SHE, CISP, and SGE in systems with slow spin relaxation. Recently, it has been shown that all three effects take place in 2D systems with hopping conductivity and pronounced spin-orbit interaction [21,48]. Impression of SHE, for example, is shown in Fig. 1. In this work, we investigate the spin-related phenomena for localized carriers, as functions of the nuclei-induced spin relaxation time and external perpendicular magnetic field.

The paper is organized as follows. In Sec. II we derive and analyze kinetic equations for the coupled charge and spin dynamics. In Sec. III we solve these equations using both numerical simulation and percolation analysis. The obtained results and their generalizations are discussed in Sec. IV and are summarized in Sec. V.

II. GENERAL THEORY

A. Phenomenology

In two-dimensional systems CISP, SGE and SHE are introduced by the following phenomenological expressions [21]:

$$\boldsymbol{s} = \hat{\boldsymbol{\sigma}}_{\mathrm{CISP}}\boldsymbol{E}, \quad \boldsymbol{j} = \hat{\boldsymbol{\sigma}}_{\mathrm{SGE}}\boldsymbol{s}, \quad \boldsymbol{\mathcal{J}} = \hat{\boldsymbol{\sigma}}_{\mathrm{SHE}}\boldsymbol{E}, \tag{1}$$

where $\boldsymbol{s}$ is the average spin polarization, $\boldsymbol{E}$ is the applied electric field, $\boldsymbol{j}$ is the current density, and $\boldsymbol{\mathcal{J}}$ is the component of

FIG. 1. Impression of SHE. The hopping of electrons (frogs) in one direction is accompanied by separation of electrons (frogs) with spins (arrows) up and down in perpendicular direction.

the spin current associated with the spin-z component (normal to the plane of the structure). The generalized conductivities $\hat{\boldsymbol{\sigma}}_{\mathrm{CISP}}$, $\hat{\boldsymbol{\sigma}}_{\mathrm{SGE}}$, and $\hat{\boldsymbol{\sigma}}_{\mathrm{SHE}}$ depend on structure parameters and external magnetic field $\boldsymbol{B}$.

We consider a semiconductor zinc-blende heterostructure grown along the [001] direction. In this case, it is useful to introduce the coordinate frame as $z \parallel [001]$, $x \parallel [1\bar{1}0]$, and $y \parallel [110]$. In this coordinate frame the Hamiltonian describing spin-orbit interaction has the form [25]

$$\mathcal{H}_{\mathrm{SO}} = \hat{\boldsymbol{\sigma}} \cdot \hat{\boldsymbol{\beta}}\boldsymbol{k} = \hat{\sigma}_x \beta_{xy} k_y + \hat{\sigma}_y \beta_{yx} k_x. \tag{2}$$

Here, $\hat{\sigma}_{x,y}$ are the Pauli matrices, $\boldsymbol{k} = -i\boldsymbol{\nabla}$, and β_{xy}, β_{yx} are two spin-orbit constants caused by both bulk- and structure-inversion asymmetry.

We assume that the external magnetic field is applied perpendicular to the structure $\boldsymbol{B} = B_z \boldsymbol{e}_z$, where $\boldsymbol{e}_z$ is the unit vector along z direction. The asymmetric heterostructures are described by C_{2v} point symmetry group. In this case, the components E_x and s_y transform according to Γ_2 representation, E_y and s_x belong to Γ_4 representation, while B_z transforms according to Γ_3. Importantly, the symmetry analysis shows the following:

(i) the diagonal components of all the generalized susceptibilities are odd in B_z,

(ii) the off-diagonal components are even in B_z.

In the particular cases of structure-inversion asymmetry dominance ($C_{\infty v}$ symmetry) and bulk-inversion asymmetry dominance (D_{2d} symmetry), the components of the tensors $\hat{\boldsymbol{\sigma}}_{\mathrm{CISP,SGE}}$ are related by

$$\sigma^{xy}_{\mathrm{CISP,SGE}} = \mp\sigma^{yx}_{\mathrm{CISP,SGE}}, \quad \sigma^{xx}_{\mathrm{CISP,SGE}} = \pm\sigma^{yy}_{\mathrm{CISP,SGE}}, \tag{3}$$

where the upper (lower) sign should be taken for $C_{\infty v}$ (D_{2d}) point symmetry. For the spin Hall effect, the following relation takes place in both cases:

$$\sigma^{xy}_{\mathrm{SHE}} = -\sigma^{yx}_{\mathrm{SHE}}, \quad \sigma^{xx}_{\mathrm{SHE}} = \sigma^{yy}_{\mathrm{SHE}}. \tag{4}$$

The structures grown along crystallographic directions other than [001] are briefly discussed in Sec. IV.

B. Derivation of the kinetic equation

In the hopping conductivity regime the electron energies are different for different localization sites. Therefore, hopping between the sites involves emission or absorption of phonons to ensure the energy conservation. The total Hamiltonian of the system can be presented as

$$\mathcal{H} = \mathcal{H}_e + \mathcal{H}_{ph} + \mathcal{H}_{e\text{-}ph}. \tag{5}$$

Here, the term $\mathcal{H}_e$ describes the Hamiltonian of the electronic system, $\mathcal{H}_{ph}$ is the phonon Hamiltonian, and $\mathcal{H}_{e\text{-}ph}$ describes the electron-phonon interaction.

The Hamiltonian describing the system of localized electrons reads as

$$\mathcal{H}_e = \sum_{i,\sigma} \epsilon_i c^\dagger_{i\sigma} c_{i\sigma} + \sum_{ij} \sum_{\sigma\sigma'} J^{\sigma\sigma'}_{ij} c^\dagger_{i\sigma} c_{j\sigma'} + \mathcal{H}_Z. \tag{6}$$

Here, $c^\dagger_{i\sigma}$ ($c_{i\sigma}$) are the creation (annihilation) operators of an electron at the site i with the spin projection $\sigma = \pm\frac{1}{2}$ on the normal to the 2D plane, z axis, and ϵ_i are the spin-independent site energies. The second term in Eq. (6) describes the spin-dependent hopping with the amplitudes $J^{\sigma\sigma'}_{ij}$. $\mathcal{H}_Z$ is the Zeeman Hamiltonian. In this and the next section we neglect the electron g factor for the sake of simplicity, thus assuming $\mathcal{H}_Z = 0$. The modification of kinetic equations accounting for the Zeeman splitting is discussed in Sec. IV.

The hopping amplitude is determined by the transfer integral

$$J^{\sigma\sigma'}_{ij} \sim \int d\boldsymbol{r}\, \Psi^*_\sigma(\boldsymbol{r} - \boldsymbol{r}_i) V(\boldsymbol{r}) \Psi_{\sigma'}(\boldsymbol{r} - \boldsymbol{r}_j), \tag{7}$$

where $V(\boldsymbol{r})$ is the potential energy including the attraction potential of sites i and j. The localized electron wave function has the asymptotic form [26]

$$\Psi_\sigma(\boldsymbol{r}) \sim \exp\left\{\frac{i}{\hbar}\int_0^r \left[\boldsymbol{p}(\boldsymbol{r}') - \frac{e}{c}\widetilde{\boldsymbol{A}}(\boldsymbol{r}')\right] d\boldsymbol{r}'\right\} \chi_\sigma. \tag{8}$$

Here, χ_σ is the basis spinor, $\boldsymbol{p}(\boldsymbol{r})$ is the imaginary quasiclassical momentum of electrons, and

$$\widetilde{\boldsymbol{A}}(\boldsymbol{r}) = \boldsymbol{A}(\boldsymbol{r}) - \frac{cm}{\hbar e}\hat{\boldsymbol{\sigma}} \cdot \hat{\boldsymbol{\beta}} \tag{9}$$

is the modified vector potential. It includes the vector potential of the applied magnetic field and the term corresponding to spin-orbit interaction. This allows us to obtain [49–52]

$$\hat{J}_{ij} = J_{ij}\hat{U}_{ij}, \tag{10a}$$

where

$$J_{ij} = J_0 e^{-r_{ij}/a_b}, \quad \hat{U}_{ij} = \exp(-i\boldsymbol{d}_{ij} \cdot \hat{\boldsymbol{\sigma}} + i\varphi_{ij}). \tag{10b}$$

Here, we neglected power-law terms in $\hat{J}_{ij}$ in comparison to the exponential dependence e^{-r_{ij}/a_b}. The spin-orbit and magnetic-field-induced phases are given by

$$\boldsymbol{d}_{ij} = \frac{m}{\hbar^2}\hat{\boldsymbol{\beta}}\boldsymbol{r}_{ij}, \quad \varphi_{ij} = \frac{e\boldsymbol{B}}{2\hbar c} \cdot (\boldsymbol{r}_i \times \boldsymbol{r}_j), \tag{10c}$$

respectively, where m is the electron effective mass, $\boldsymbol{r}_i$ are the coordinates of the sites in the 2D plane, $\boldsymbol{r}_{ij} = \boldsymbol{r}_i - \boldsymbol{r}_j$, a_b is the localization length [53], and we have used the Coulomb gauge. J_0 is a real constant of the order of the binding energy. In general case J_0 and a_b are even functions of the magnetic field [53].

The phonon Hamiltonian has the form

$$\mathcal{H}_{ph} = \sum_{\boldsymbol{q}} \hbar\Omega_{\boldsymbol{q}} b^\dagger_{\boldsymbol{q}} b_{\boldsymbol{q}}, \tag{11}$$

where $\hbar\Omega_{\boldsymbol{q}}$ is the energy of the phonon with the wave vector $\boldsymbol{q}$, and $b_{\boldsymbol{q}}$ ($b^\dagger_{\boldsymbol{q}}$) is the corresponding annihilation (creation)

operator. The Hamiltonian of the electron-phonon interaction reads as

$$\mathcal{H}_{e\text{-}ph} = \sum_{i,\sigma,\boldsymbol{q}} v_q (e^{i\boldsymbol{q}\boldsymbol{R}_i} b_{\boldsymbol{q}} + e^{-i\boldsymbol{q}\boldsymbol{R}_i} b^\dagger_{\boldsymbol{q}}) c^\dagger_{i\sigma} c_{i\sigma} \tag{12}$$

with v_q being the electron-phonon interaction constants. The spin dependence of electron-phonon interaction is negligible.

After the canonical transformation [54,55], the total Hamiltonian can be presented as

$$\mathcal{H} = \sum_{i,\sigma} \epsilon_i c^\dagger_{i\sigma} c_{i\sigma} + \sum_{\boldsymbol{q}} \hbar\Omega_q b^\dagger_{\boldsymbol{q}} b_{\boldsymbol{q}} + \sum_{i,j,\sigma,\sigma'} V^{\sigma\sigma'}_{ij} c^\dagger_{i\sigma} c_{j\sigma'}, \tag{13}$$

where $V^{\sigma\sigma'}_{ij} = J^{\sigma\sigma'}_{ij} Q_{ij}$ with

$$Q_{ij} = \exp\left\{ -\sum_{\boldsymbol{q}} \gamma_q \left[\left(e^{i\boldsymbol{q}\boldsymbol{r}_i} - e^{i\boldsymbol{q}\boldsymbol{r}_j} \right) b_{\boldsymbol{q}} + \text{H.c} \right] \right\}, \tag{14}$$

$\gamma_q = v_q/(\hbar\Omega_q)$, and we have neglected the renormalization of ϵ_i.

The aim of microscopic theory is to to derive the kinetic equation. For the sake of simplicity, we limit ourselves to the lowest orders of perturbation theory in the electron-phonon and spin-orbit interactions. Provided the concentration of charge carriers n is inferior by far than the concentration of localization sites n_s, one can neglect correlation effects. Additionally, under assumption that the concentration of localization sites is much smaller than the inverse localization length squared, $n_s \ll a_b^{-2}$, we will use the onsite spin density matrices $\hat{\rho}_i$. The master equation can be presented as

$$\frac{d\hat{\rho}_i}{dt} = \sum_k \frac{d\hat{\rho}^{(k)}_i}{dt}, \tag{15}$$

where the sum runs over the orders of perturbation theory in the hopping amplitude.

The first nonvanishing term is the second-order contribution

$$\frac{d\hat{\rho}^{(2)}_i}{dt} = \sum_m \frac{\pi}{\hbar} \langle \delta(E_n - E_m)(2\hat{V}_{nm}\hat{\rho}_j\hat{V}_{mn} - \hat{\rho}_i\hat{V}_{nm}\hat{V}_{mn} - \hat{V}_{nm}\hat{V}_{mn}\hat{\rho}_i)\rangle. \tag{16}$$

Here, n and m denote the states of the electron-phonon system where the given electron is localized at sites i and j, respectively, and the angular brackets denote averaging over the phonon bath state. The contribution $\hat{\rho}^{(2)}_i$ describes hopping and spin rotations. Since

$$\hat{V}_{nm}\hat{V}_{mn} = J^2_{ij}\hat{1}\, Q_{ij} Q_{ji}, \tag{17}$$

where $\hat{1}$ denotes the 2×2 unit matrix, the outgoing term in the second order is the same for all spin orientations. Accordingly, the second-order contribution can be presented as

$$\frac{d\hat{\rho}^{(2)}_i}{dt} = \sum_j \left(-\frac{\hat{\rho}_i}{\tau_{ji}} + \frac{\hat{U}_{ij}\hat{\rho}_j\hat{U}_{ji}}{\tau_{ij}} \right), \tag{18}$$

with $\hat{U}_{ij}$ being the unitary spin rotation operator (10) and τ_{ji} being the hopping time from the site i to j. In the lowest (second) order in the electron-phonon interaction the hopping time is given by

$$\frac{1}{\tau_{ji}} = \frac{2\pi}{\hbar} J^2_{ij} 2\gamma^2_{q_{ij}} D(|\epsilon_{ij}|)[N_{|\epsilon_{ij}|} + \Theta(\epsilon_{ij})], \tag{19}$$

where $\epsilon_{ij} = \epsilon_i - \epsilon_j$, q_{ij} is the phonon wave vector corresponding to this energy, $\Theta(\epsilon)$ is the Heaviside function, $D(\epsilon)$ stands for the phonon density of states, and $N_\epsilon = 1/[\exp(\epsilon/k_BT) - 1]$ is the occupation of the phonon state with k_B and T being the Boltzmann constant and temperature, respectively. This result can be conveniently obtained using the hopping diagrams introduced in Ref. [21]. The multiplier 2 reflects the fact that the phonon can be emitted either at site i or j. Note that, due to the energy difference, $\tau_{ji} \neq \tau_{ij}$. As it is commonly accepted, we neglect simultaneous hops of two and more electrons.

In what follows, we derive all the other terms of the kinetic equation in the lowest nonvanishing order in spin-orbit interaction. The effective frequency of spin precession during the hop is accordingly given by $\boldsymbol{\Omega}_{ij} = 2\boldsymbol{d}_{ij}/\tau_{ij}$ provided $|\boldsymbol{\Omega}_{ij}\tau_{ij}| \ll 1$.

The third-order contribution to the master equation has the form

$$\frac{d\hat{\rho}^{(3)}_i}{dt} = -\frac{4\pi}{\hbar} \sum_{m,l} \left\langle \delta(E_n - E_m) \left\{ \pi\, \mathrm{Im}(\hat{V}_{nm}\hat{\rho}_j\hat{V}_{ml}\hat{V}_{ln})\delta(E_n - E_l) + \frac{\mathrm{Re}[\hat{\rho}_i\,\mathrm{Re}(\hat{V}_{nm}\hat{V}_{ml}\hat{V}_{ln}) - \hat{V}_{nm}\hat{\rho}_j\hat{V}_{ml}\hat{V}_{ln}]}{E_n - E_l} \right\} \right\rangle, \tag{20}$$

where we have introduced the notations $\mathrm{Re}\, O \equiv (O + O^\dagger)/2$ and $\mathrm{Im}\, O \equiv (O - O^\dagger)/(2i)$. It can be rewritten in a form similar to Eq. (18):

$$\frac{d\hat{\rho}^{(3)}_i}{dt} = \sum_{jk} \left\{ \mathrm{Re}\left[\frac{\hat{U}_{ij}\hat{\rho}_j\hat{U}_{jk}\hat{U}_{ki}}{\tau_{ikj}} - \frac{\hat{\rho}_i\,\mathrm{Re}(\hat{U}_{ij}\hat{U}_{jk}\hat{U}_{ki})}{\tau_{jki}} \right] - \frac{\mathrm{Im}(\hat{U}_{ij}\hat{\rho}_j\hat{U}_{jk}\hat{U}_{ki})}{\tau'_{ikj}} \right\}, \tag{21}$$

where

$$\frac{1}{\tau_{ikj}} = \frac{1}{\tau_{ij}} \frac{J_{ik}J_{kj}}{2J_{ij}} \left(\frac{1}{\epsilon_i - \epsilon_k} + \frac{1}{\epsilon_j - \epsilon_k} \right), \tag{22a}$$

$$\frac{1}{\tau'_{ikj}} = \frac{\hbar}{4} \left(\frac{J_{ij}}{J_{kj}J_{ki}\tau_{ik}\tau_{kj}} + \frac{J_{jk}}{J_{ij}J_{ki}\tau_{ki}\tau_{ij}} + \frac{J_{ik}}{J_{ij}J_{kj}\tau_{ij}\tau_{kj}} \right). \tag{22b}$$

These expressions can be also directly obtained from the diagrammatic approach [21]. We note that the rate $1/\tau_{ikj}$ describes emission/absorption of one phonon. These rates contribute to the interference mechanism of magnetoresistance [56,57]. The rate $1/\tau'_{ikj}$ describes interaction with at least two phonons. The corresponding processes lead to the hopping Hall effect [49,58]. For our purposes, it is important

to keep both contributions because they have different symmetry.

It is convenient to present the onsite density matrix in the form

$$\hat{\rho}_i = \frac{n_i}{2}\hat{1} + \hat{\boldsymbol{\sigma}} \cdot \boldsymbol{S}_i, \tag{23}$$

where n_i is the occupancy of site i, and $\boldsymbol{S}_i$ is the corresponding spin. Substitution of this expression into Eqs. (15), (18), and (21) yields a system of coupled kinetic equations:

$$\dot{n}_i = \sum_j I_{ij} + \sum_j (\boldsymbol{\Lambda}_{ij} \cdot \boldsymbol{S}_j - \boldsymbol{\Lambda}_{ji} \cdot \boldsymbol{S}_i), \tag{24a}$$

$$\dot{\boldsymbol{S}}_i + \sum_j \boldsymbol{S}_j \times \boldsymbol{\Omega}_{ij} + \frac{\boldsymbol{S}_i}{\tau_s} = \sum_j \boldsymbol{I}^s_{ij} + \sum_j (\boldsymbol{G}_{ij} n_j + \boldsymbol{G}_{ji} n_i). \tag{24b}$$

Here,

$$I_{ij} = \frac{n_j}{\tau_{ij}} - \frac{n_i}{\tau_{ji}} \tag{25}$$

is the particle flow between sites i and j. Assuming that spin relaxation is mainly governed by the onsite hyperfine interaction, we phenomenologically introduced the spin relaxation time τ_s. We note that the hopping time τ_{ij} as well as the spin relaxation time τ_s can be anisotropic, which is disregarded in Eqs. (24). The spin current flowing from the site j to the site i is a sum of two contributions

$$\boldsymbol{I}^s_{ij} = \frac{\boldsymbol{S}_j}{\tau_{ij}} - \frac{\boldsymbol{S}_i}{\tau_{ji}} + \boldsymbol{W}_{ij} n_j - \boldsymbol{W}_{ji} n_i. \tag{26}$$

The first two terms describe spin diffusion, while the latter terms arise due to a difference in spin-conserving tunneling rates for electrons with spins oriented along ($\uparrow$) and opposite ($\downarrow$) to the axis α: $W^\alpha_{ij} = (W_{\uparrow\uparrow} - W_{\downarrow\downarrow})/2$. Similarly, $G^\alpha_{ij} = (W_{\uparrow\downarrow} - W_{\downarrow\uparrow})/2$ describes spin generation, where $W_{\uparrow\downarrow}$ and $W_{\downarrow\uparrow}$ denote the tunneling rates with the spin flips between the corresponding orientations. The spin-galvanic coefficient can be presented as $\Lambda^\alpha_{ij} = 2(W_{\uparrow\uparrow} + W_{\downarrow\uparrow} - W_{\downarrow\downarrow} - W_{\uparrow\downarrow})$. Therefore, we obtain a general relation

$$\boldsymbol{\Lambda}_{ij} = 4(\boldsymbol{W}_{ij} - \boldsymbol{G}_{ij}). \tag{27}$$

The kinetic coefficients $\mathcal{K}_{ij}$ ($\mathcal{K} = \boldsymbol{\Lambda}, \boldsymbol{G}, \boldsymbol{W}$) in Eq. (24) are equal to sums over the auxiliary sites $\mathcal{K}_{ij} = \sum_k \mathcal{K}_{ijk}$, and the relation (27) holds for $\mathcal{K}_{ijk}$ as well. These expressions demonstrate that CISP, SGE, and SHE arise only taking into account hopping between three sites, i.e., triads should be considered. From the ingoing contributions in Eq. (21) we obtain that

$$\boldsymbol{\Gamma}_{ikj} \equiv \boldsymbol{G}_{ikj} + \boldsymbol{W}_{ikj} = \alpha_{xy}\alpha_{yx}\left[\frac{2}{3}\boldsymbol{A}_{ikj} \times \hat{\boldsymbol{\alpha}}(\boldsymbol{r}_{ij} + \boldsymbol{r}_{ik}) - \boldsymbol{A}_{ikj}\right]\left(\frac{\cos\varphi_{ikj}}{\tau'_{ikj}} + \frac{\sin\varphi_{ikj}}{\tau_{ikj}}\right), \tag{28a}$$

$$\boldsymbol{\Lambda}_{ikj} = 4\alpha_{xy}\alpha_{yx}\left[\frac{2}{3}\boldsymbol{A}_{ikj} \times \hat{\boldsymbol{\alpha}}(\boldsymbol{r}_{jk} + \boldsymbol{r}_{ji}) - \boldsymbol{A}_{ikj}\right] \times \left(\frac{\cos\varphi_{ikj}}{\tau'_{ikj}} + \frac{\sin\varphi_{ikj}}{\tau_{ikj}}\right), \tag{28b}$$

where $\boldsymbol{A}_{ikj} = \boldsymbol{r}_{ki} \times \boldsymbol{r}_{ij}/2$ is the oriented area of the triad, $\hat{\boldsymbol{\alpha}} = m\hat{\boldsymbol{\beta}}/\hbar^2$, and

$$\varphi_{ikj} = \varphi_{ij} + \varphi_{jk} + \varphi_{ki} = 2\pi\frac{\Phi_{ikj}}{\Phi_0} \tag{29}$$

with $\Phi_{ikj} = \boldsymbol{B} \cdot \boldsymbol{A}_{ikj}$ being the magnetic flux through the triad (see inset in Fig. 5) and $\Phi_0 = 2\pi\hbar c/|e|$ being the magnetic flux quantum. Using the relation (27) one finds

$$\boldsymbol{G}_{ikj} = \alpha_{xy}\alpha_{yx}\boldsymbol{A}_{ikj} \times \hat{\boldsymbol{\alpha}}\boldsymbol{r}_{ij}\left(\frac{\cos\varphi_{ikj}}{\tau'_{ikj}} + \frac{\sin\varphi_{ikj}}{\tau_{ikj}}\right), \tag{30a}$$

$$\boldsymbol{W}_{ikj} = \alpha_{xy}\alpha_{yx}\left[\frac{\boldsymbol{A}_{ikj}}{3} \times \hat{\boldsymbol{\alpha}}(\boldsymbol{r}_{jk} + \boldsymbol{r}_{ik}) - \boldsymbol{A}_{ikj}\right] \times \left(\frac{\cos\varphi_{ikj}}{\tau'_{ikj}} + \frac{\sin\varphi_{ikj}}{\tau_{ikj}}\right). \tag{30b}$$

We see that the kinetic coefficients oscillate with magnetic field, and the period of oscillations is determined by the triad area A_{ikj}.

We note that the phase related with the spin-orbit interaction is equivalent to the dynamical phase factor:

$$\hat{\boldsymbol{\sigma}}\boldsymbol{d}_{ij} = \frac{1}{\hbar}\int \hat{\boldsymbol{\sigma}}\hat{\boldsymbol{\beta}}\boldsymbol{k}_{ij}(t)dt, \tag{31}$$

where the wave vector $\boldsymbol{k}_{ij}(t)$ describes propagation of an electron from site j to i. In the same time, the Aharonov-Bohm phase φ_{ij} is known to be geometric or Berry phase [59,60].

C. General properties of kinetic equation

Summation of Eq. (24b) over all sites yields the total spin generation rate in the form

$$\sum_i \dot{\boldsymbol{S}}_i = \sum_{ijk}{}' \boldsymbol{\Upsilon}_{ikj} + \sum_{ij} \boldsymbol{\Omega}_{ij} \times \boldsymbol{S}_j - \sum_i \frac{\boldsymbol{S}_i}{\tau_s}, \tag{32}$$

where the prime denotes that each pair (j, k) should be taken only once, and

$$\boldsymbol{\Upsilon}_{ikj} = \boldsymbol{\Gamma}_{ikj} n_j + \boldsymbol{\Gamma}_{ijk} n_k - \frac{n_i}{4}(\boldsymbol{\Lambda}_{jki} + \boldsymbol{\Lambda}_{kji}). \tag{33}$$

Note that the terms with spin-conserving tunneling rates ($\boldsymbol{W}_{ij}$) in $\boldsymbol{\Gamma}_{ij}$ and $\boldsymbol{\Lambda}_{ij}$ cancel each other, but we keep them for the future convenience.

In thermal equilibrium the rate $\boldsymbol{\Upsilon}_{ikj}$ vanishes, and the spin polarization is absent. This can be explicitly shown with the help of relations

$$\frac{n_j}{\tau_{ij}} = \frac{n_i}{\tau_{ji}}, \quad \frac{n_j}{\tau_{ikj}} = \frac{n_i}{\tau_{jki}}, \quad \frac{n_j}{\tau'_{ikj}} = \frac{n_k}{\tau'_{ijk}}, \quad \tau'_{ikj} = \tau'_{kij}. \tag{34}$$

The first of these relations follows from Eq. (19) and represents the detailed balance equation $I_{ij} = 0$ in thermal equilibrium, while the rest follow directly from Eqs. (22).

These expressions along with the definitions Eq. (28) yield

$$\Lambda'_{jki}+\Lambda'_{kji}=0,\quad \Gamma'_{ikj}n_j+\Gamma'_{ijk}n_k=0,$$
$$\Gamma''_{ikj}n_j-\frac{1}{4}\Lambda''_{jki}n_i=0,\quad \Gamma''_{ijk}n_k-\frac{1}{4}\Lambda''_{kji}n_i=0, \quad (35)$$

where one and two primes denote the even in B_z contributions proportional to $1/\tau'_{ikj}$ and the odd in B_z ones proportional to $1/\tau_{ikj}$, respectively [see Eqs. (28)]. Combining all together one finds $\Upsilon_{ikj}=0$ in thermal equilibrium, as expected. In close to equilibrium conditions we obtain

$$\Upsilon_{ikj}=\Gamma'_{ikj}\tau_{kj}I_{kj}+\Gamma''_{ikj}\tau_{ij}I_{ij}+\Gamma''_{ijk}\tau_{ik}I_{ik}. \quad (36)$$

This expression is similar to "Hall source" in the theory of hopping Hall effect [58].

The average spin evolution follows from Eq. (32):

$$\dot{\boldsymbol{s}}=\frac{1}{nA}\sum_i\dot{\boldsymbol{S}}_i=\frac{1}{nA}\sum_{ij}(2\boldsymbol{G}_{ij}n_j+\boldsymbol{\Omega}_{ij}\times\boldsymbol{S}_j)-\frac{\boldsymbol{s}}{\tau_s}, \quad (37)$$

where A is the total area of the sample. This expression differs from Eq. (32) by omission of spin-conserving tunneling terms. It can be conveniently rewritten introducing the total spin current

$$\mathcal{J}=\frac{1}{2A}\sum_{ij}\boldsymbol{r}_{ij}I^{s,z}_{ij} \quad (38)$$

as follows [6,21]:

$$\dot{\boldsymbol{s}}=-\frac{2}{n}\boldsymbol{e}_z\times\hat{\boldsymbol{\alpha}}\mathcal{J}-\frac{\boldsymbol{s}}{\tau_s}, \quad (39)$$

with $\boldsymbol{e}_z$ being a unit vector along the z axis. We remind that we restrict ourselves only to the lowest (third) order in spin-orbit interaction. Defined in this way the spin current vanishes in thermodynamic equilibrium. One can separate two qualitatively different contributions to the spin current: $\mathcal{J}_{\rm diff}$ and $\mathcal{J}_{\rm dr}$, as the two first and two latter terms in Eq. (26). Provided the electric field is applied to the structure along x direction the sum of the two contributions in the perpendicular direction is related only to the spin relaxation:

$$\mathcal{J}_y=\frac{1}{\tau_s A}\sum_i y_i S^z_i. \quad (40)$$

The spin current in the longitudinal (x) direction can be nonzero even without spin relaxation as a product of spin polarization and electric current. We remind that, in accordance with the symmetry analysis performed in Sec. II A, the odd and even in B_z contributions to spin orientation and spin current averaged over disorder are perpendicular to each other.

It follows from Eq. (37) in the steady state that the CISP conductivity can be presented as

$$\hat{\boldsymbol{\sigma}}_{\rm CISP}=[f(n_s,\tau_s)+g(n_s,\tau_s)\boldsymbol{e}_z\times]\,{\rm Tr}(\hat{\boldsymbol{\beta}}^2)\hat{\boldsymbol{\beta}}^T\mathcal{P}\tau_s. \quad (41)$$

Here,

$$\mathcal{P}=\left(\frac{ma_b}{\hbar^2}\right)^3\frac{2\hbar n_s a_b}{enJ_0\tau_0\rho}, \quad (42)$$

ρ is the resistivity, and τ_0 is the characteristic time for the distance $\sim a_b$.[1] The dimensionless functions $f(n_s,\tau_s)$ and $g(n_s,\tau_s)$ are even and odd in B_z, respectively, as follows from the symmetry analysis presented in Sec. II A.

The spin-galvanic current can be similarly obtained from the kinetic equation (24a). The calculation yields the following result for the SGE response:

$$\hat{\boldsymbol{\sigma}}_{\rm SGE}=[f(n_s,\tau_s)-g(n_s,\tau_s)\boldsymbol{e}_z\times]4\,{\rm Tr}(\hat{\boldsymbol{\beta}}^2)\hat{\boldsymbol{\beta}}^T\mathcal{P}k_BTn. \quad (43)$$

Here, the functions f and g coincide with those for CISP [Eq. (41)] as follows from the Onsager relation [12,21,61].

The spin Hall conductivity can be deduced from Eqs. (39) and (41):

$$\hat{\boldsymbol{\sigma}}_{\rm SHE}=-[f(n_s,\tau_s)+g(n_s,\tau_s)\boldsymbol{e}_z\times]\hat{\boldsymbol{\beta}}^T(\boldsymbol{e}_z\times\hat{\boldsymbol{\beta}})\frac{\hbar^2n\mathcal{P}}{m}. \quad (44)$$

We stress that, in the inhomogeneous system under study, the drift and diffusion currents are always interconnected. Therefore, the spin Hall conductivity describes the *total* spin current induced by the applied electric field. The constant drift spin current, leading to spin separation, can be found formally from Eq. (44) in the limit $\tau_s\to 0$ when the diffusion spin current vanishes.

III. DISORDER AVERAGING

The above analysis provides microscopic equations that describe CISP, SGE, and SHE in the hopping regime. Ultimately, we are interested in the macroscopic susceptibilities introduced in Eqs. (1). However, in the disordered system the link between microscopic expressions and macroscopic parameters is not straightforward due to an exponential distribution of the hopping times.

Equations (41)–(44) express macroscopic susceptibilities through the dimensionless functions $f(n_s,\tau_s)$ and $g(n_s,\tau_s)$. In this section we study in detail the even in magnetic field effects that are described by $f(n_s,\tau_s)$. In what follows, for brevity we call the function $f(n_s,\tau_s)$ the *spin susceptibility*. As it is shown in the previous section, the kinetic coefficients (28) and (30) oscillate with magnetic field. In this section we demonstrate that these oscillations are strongly modified in a macroscopic system due to the disorder.

We consider the system with dominant spatial disorder. So, we assume that the energy disorder $|\epsilon_i-\epsilon_j|$ is small or comparable to the temperature. In this case, we can neglect the dependence of hopping times τ_{ij} on energies in comparison to the strong dependence on site positions. Also we limit ourselves to Ohmic regime. In the analysis of the magnetic-field dependence of the spin susceptibility we neglect for simplicity the dependencies of τ_0 and a_b on B_z as well as magnetoresistance.

[1] Here we define $\mathcal{P}$ as a value two times larger than in Ref. [21].

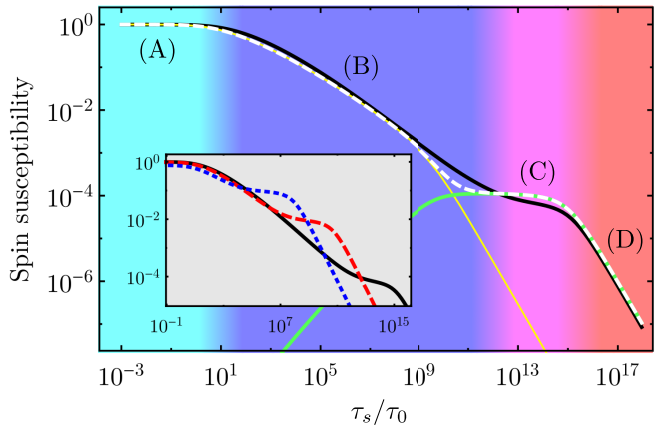

FIG. 2. The spin susceptibility $f(n_s, \tau_s)$ calculated numerically for $n_s a_b^2 = 0.01$ (black curve) and its analytical approximation (56) (white dashed curve) with the parameters $\gamma = 1$ and $D = 0.5 \times 10^{-8} a_b^2/\tau_0$. The background colors distinguish the four regimes (A), (B), (C), and (D) discussed in the text. Yellow and green curves show the two contributions (58) and (66) to the spin current in the percolation model. The inset shows the same black solid curve and the spin susceptibility calculated for $n_s a_b^2 = 0.3$ (red dashed curve) and 0.1 (blue dotted curve).

A. Numerical simulation

We have performed a numerical simulation of coupled charge and spin dynamics described by Eqs. (24). As it is mentioned above, we have assumed that the spatial disorder dominates over energy disorder. In this case, the hopping time in each pair (ij) has the form

$$\tau_{ij} = \tau_{ji} = \tau_0 e^{2r_{ij}/a_b} \tag{45}$$

with τ_0 being a constant. The conductivity of the system was analyzed using Miller-Abrahams random resistor network where each pair is replaced by a resistor with the resistivity $R_{ij} = nk_BT\tau_{ij}/(e^2 n_s)$ [53]. In this model, a numerical solution of a set of Kirchhoff equations yielded the particle flows I_{ij} for each pair of sites. In the next step, the spin generation rates $\boldsymbol{\Upsilon}_{ijk}$ were calculated using Eqs. (36). Then, the steady-state spin density was found from Eqs. (24b). At this step we neglected spin generation rate $\boldsymbol{G}_{ij}$ and spin precession $\boldsymbol{\Omega}_{ij}$ because they are proportional to the third power of spin-orbit constants. And, finally, the spin current was calculated using Eq. (40). Comparison of the result with Eq. (44) yielded the spin susceptibility $f(n_s, \tau_s)$. We have performed numerical simulations for $N_s = 512 \times 10^3$ localization sites with the Poisson distribution, and we have checked that the difference between the three realizations of the disorder was less than 1%.

The dependence of the spin susceptibility on the spin relaxation time at zero magnetic field is shown in Fig. 2 by the black line for $n_s a_b^2 = 0.01$. One can distinguish four regimes in the dependence of the spin susceptibility on the spin relaxation time which are shown by different background colors in Fig. 2. For small τ_s we find that f tends to 1 [cyan region, regime (A)]. When τ_s increases, in the blue region, the spin susceptibility decays approximately as $1/\sqrt{\tau_s}$ [regime (B)]. This decrease stops at a certain value, and in the magenta region of τ_s the spin susceptibility hardly changes [regime (C)]. Finally, for large enough spin relaxation time, f decays as $1/\tau_s$ [red region, regime (D)]. As it is shown in the inset, the second (blue) region narrows down with increase of the concentration n_s.

We show the numerically calculated distribution of generated spin in Fig. 3. Here the color scale is arbitrary. It can be seen that in the regime (A) all the generated spin is localized at close pairs with small separations. In the regime (B), the spin is still localized on rare sites but the separation of the up and down spins is larger. In the regime (C), the generated spin covers entire regions of the sample indicating spin diffusion with a finite length l_s. Finally, in the regime (D) the spin polarization is distributed over the whole sample due to the large spin diffusion length $l_s > L$, with $L = \sqrt{N_s/n_s}$ being the sample size.

Figure 4 demonstrates the magnetic-field dependence of the normalized spin susceptibility as a function of two parameters τ_s/τ_0 and B_z/B_0, where $B_0 = \Phi_0/(2\pi a_b^2)$. One can see that the dependence $f(B_z)$ can have either one or multiple changes of sign depending on the relation between the spin relaxation and the hopping times.

B. Percolation analysis

In this section we develop an analytical theory to describe the dependence of the spin susceptibility on the spin relaxation time and magnetic field. This is possible in the limit of strong disorder $n_s a_b^2 \ll 1$, when the percolation theory can be applied [53]. The presented results are qualitative, but they are in a good agreement with numerical simulations.

First, let us briefly summarize the main facts of percolation theory for system conductivity [53]. As mentioned in the previous subsection, the ensemble of localization sites can be mapped onto the Miller-Abrahams network of resistors with the resistivities

$$R_{ij} \propto \tau_{ij}. \tag{46}$$

Due to the exponentially broad distribution of the hopping times, the current mainly flows in a percolation cluster. It includes only resistors with

$$R_{ij} \lesssim R_{\rm perc} = \frac{k_BTn\tau_0}{n_s e^2} \exp(2r_c/a_b), \tag{47}$$

where $r_c = 2\sqrt{\eta_c/\pi} n_s^{-1/2}$ is the percolation distance. For the 2D system under study, the percolation threshold is $\eta_c \approx 1.128$ [62]. We note that the system resistivity can be estimated as $\rho \sim R_{\rm perc}$. Despite the strong disorder, the system can be considered as a homogeneous one with a usual diffusive conductivity on the length scale exceeding the correlation length

$$L_{\rm cor} = n_s^{-1/2} (r_c/a_b)^\nu, \tag{48}$$

with the critical exponent $\nu \approx 1.3$ [62].

Now, we turn to the analysis of the spin susceptibility. Similarly to the numerical simulation discussed above, its calculation consists of two steps. In the first step, a distribution of electric currents in the system is determined. In the second step, one can analyze the spin-related phenomena on the basis of Eqs. (24b) and (36) with the known particle fluxes I_{ij}. The analysis of the spin susceptibility can be conveniently

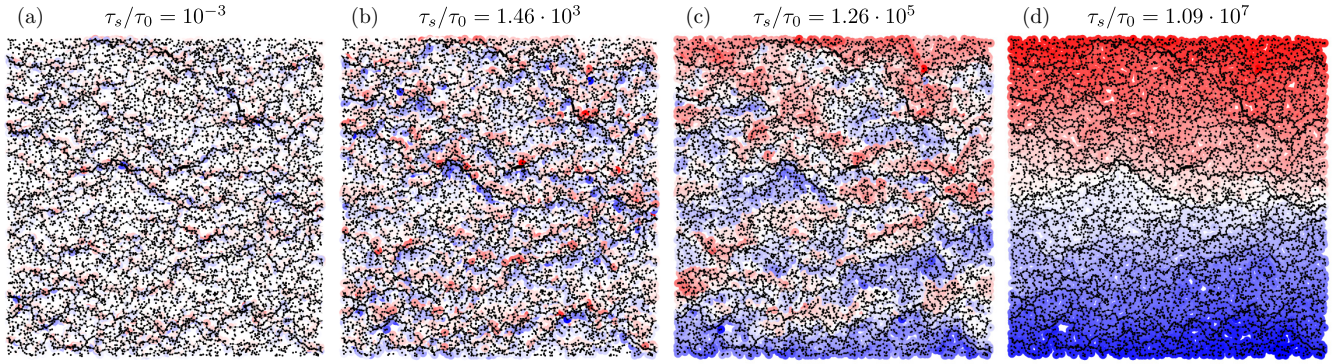

FIG. 3. Spatial distribution of $S_{i,z}$ for different spin relaxation times in zero magnetic field. The four panels (a)–(d) correspond to the regimes (A)–(D). The red color corresponds to $S_{i,z} > 0$ and blue color to $S_{i,z} < 0$. The color scale is arbitrary. The black lines show the particle fluxes between the sites: the thicker is the line, the larger is the flux. Parameters of the calculation are $n_s a_b^2 = 0.1$ and $N_s = 10^4$.

done considering SHE, so we again reduce the kinetic equations (24) to the second order in spin-orbit interaction. The corresponding equations for spin dynamics have the form

$$\dot{\mathbf{S}}_i + \frac{\mathbf{S}_i}{\tau_s} + \sum_j \frac{\mathbf{S}_i - \mathbf{S}_j}{\tau_{ij}} = \alpha_{xy}\alpha_{yx} \sum_{jk}{}' \mathbf{A}_{ikj} \frac{\tau_{jk}\cos\varphi_{ikj}}{\tau'_{ikj}} I_{jk}, \tag{49}$$

where the prime after the sum indicates that each pair (jk) should be taken only once. Note that only the z component of these equations is nonzero, which corresponds to SHE effect under study. Here, we have neglected the odd in B_z terms in the right-hand side because we are aimed only at the description of the even in magnetic-field spin susceptibility $f(n_s, \tau_s)$.

The inhomogeneous part of Eqs. (49) is related to the triads of sites along the percolation cluster where the particle flux is nonzero. Since Eqs. (49) are linear, the triads can be considered separately. Let us discuss one of these triads (ijk). We separate the contributions to the total spin current [Eq. (40)] from this particular triad, and from all the others, which we model by a diffusive medium as $\tilde{S}^{(ijk)}(\boldsymbol{r})$. It is assumed that the spin polarization can escape the triad with the rate $1/\tau_d$, and the income of spin polarization from the diffusive medium to the triad under consideration is negligible. The corresponding steady-state spins at the sites satisfy the equations

$$\begin{aligned}
&\frac{\tilde{S}_i^{(ijk)}}{\tau'_s} - \frac{\tilde{S}_k^{(ijk)} - \tilde{S}_i^{(ijk)}}{\tau_{ik}} - \frac{\tilde{S}_j^{(ijk)} - \tilde{S}_i^{(ijk)}}{\tau_{ij}} = I_{kj}\tau_{kj}\Gamma^{(0)}_{ijk},\\
&\frac{\tilde{S}_j^{(ijk)}}{\tau'_s} - \frac{\tilde{S}_k^{(ijk)} - \tilde{S}_j^{(ijk)}}{\tau_{jk}} - \frac{\tilde{S}_i^{(ijk)} - \tilde{S}_j^{(ijk)}}{\tau_{ij}} = I_{ik}\tau_{ik}\Gamma^{(0)}_{ijk},\\
&\frac{\tilde{S}_k^{(ijk)}}{\tau'_s} - \frac{\tilde{S}_i^{(ijk)} - \tilde{S}_k^{(ijk)}}{\tau_{ik}} - \frac{\tilde{S}_j^{(ijk)} - \tilde{S}_k^{(ijk)}}{\tau_{jk}} = -I_{ij}\tau_{ij}\Gamma^{(0)}_{ijk},
\end{aligned} \tag{50}$$

where $\Gamma^{(0)}_{ijk} = \alpha_{xy}\alpha_{yx}A^z_{ijk}\cos\varphi_{ikj}/\tau'_{ijk}$,

$$\frac{1}{\tau'_s} = \frac{1}{\tau_s} + \frac{1}{\tau_d}.$$

The diffusion equation in the medium has the form

$$\begin{aligned}
&\frac{\tilde{S}^{(ijk)}(\boldsymbol{r})}{\tau_s} - D\Delta\tilde{S}^{(ijk)}(\boldsymbol{r})\\
&\quad = \frac{1}{\tau_d}\left[\tilde{S}_i^{(ijk)}\delta(\boldsymbol{r}_i) + \tilde{S}_j^{(ijk)}\delta(\boldsymbol{r}_j) + \tilde{S}_k^{(ijk)}\delta(\boldsymbol{r}_k)\right]
\end{aligned} \tag{51}$$

with D being the spin diffusion coefficient. We note that

$$\tilde{S}_i^{(ijk)} + \tilde{S}_j^{(ijk)} + \tilde{S}_k^{(ijk)} = 0 \tag{52}$$

since we limit ourselves to the study of spin separation and neglect CISP here. The total contribution of the given triad to the total spin current has the form

$$\mathcal{J}_{ijk} = \mathcal{J}^{\text{triad}}_{ijk} + \mathcal{J}^{\text{med}}_{ijk}, \tag{53}$$

where

$$\mathcal{J}^{\text{triad}}_{ijk} = \frac{1}{\tau_s}\left(y_i\tilde{S}_i^{(ijk)} + y_j\tilde{S}_j^{(ijk)} + y_k\tilde{S}_k^{(ijk)}\right) \tag{54}$$

and

$$\mathcal{J}^{\text{med}}_{ijk} = \frac{1}{\tau_s}\int d\boldsymbol{r}\, y\, \tilde{S}^{(ijk)}(\boldsymbol{r}). \tag{55}$$

The net spin current is presented as

$$\mathcal{J}_y = \frac{1}{A}\sum_{ijk}{}' \mathcal{J}_{ijk}, \tag{56}$$

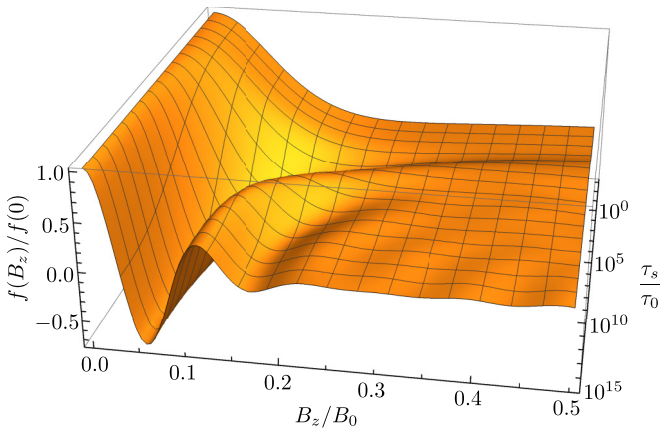

FIG. 4. Dependence of the normalized spin susceptibility on τ_s and B_z for $n_s a_b^2 = 0.01$.

where the prime after the sum indicates that each triad (ijk) should be taken only once. These equations allow one to describe the dependence of the spin susceptibility on the spin relaxation time and magnetic field shown in Figs. 2 and 4.

1. Zero magnetic field

First, we analyze the spin susceptibility at zero magnetic field. The particle flux in each branch of the percolation cluster has the same order of magnitude $I_{\rm perc}$. In a 2D system it can be estimated as $I_{\rm perc} \sim jL_{\rm cor}/e$, where we remind that j is the current density. In a given triad, $I_{\rm perc}$ is divided between the current in pairs I_{ij}, I_{jk}, and I_{ki} in accordance with the resistivities (46). This defines the right-hand side in Eqs. (50). The solution of these equations yields the contribution (54) of the triad to the total spin current. It turns out that it has a very strong dependence on the geometry of the triangle formed by the three sites under study. The maximum value of this contribution dominates the spin Hall effect.

At very short spin relaxation times $\tau_s < \tau_0$, in the regime (A), the maximum is reached in the smallest triangles. In this regime $\mathcal{J}_{\rm diff}$ can be neglected. Therefore, $\mathcal{J} = \mathcal{J}_{\rm dr}$, and the spin susceptibility is independent of τ_s in this case.

For longer spin relaxation times $\tau_s > \tau_0$, regimes (B)–(D), the maximum is reached when the sites i, j, and k form an equilateral triangle (see Appendix A). The contribution of the triangle with $r_{ij} = r_{ik} = r_{jk} = r$ to the spin current can be expressed as follows:

$$\mathcal{J}_0(r) = -I_{\rm perc}\frac{3\hbar\alpha_{xy}\alpha_{yx}r^3\tau_s'}{16J_0\tau_0\tau_s}\frac{e^{r/a_b}}{e^{2r/a_b}+3\tau_s'/\tau_0}. \tag{57}$$

The side of triangle r is arbitrary in Eq. (57). The triad contribution to the total spin current can be written in the form

$$\mathcal{J}^{\rm triad} = \int_0^{r_c} dr\, p(r)\mathcal{J}_0(r), \tag{58}$$

where $p(r)$ is proportional to the distribution function of the triangles of the size r along the percolation cluster. We assume that it has the form

$$p(r) \propto 1/r^{\gamma}, \tag{59}$$

where γ is a constant. This dependence with $\gamma > 0$ reflects the fact that the probability to find an equilateral triangle with a side $r \lesssim r_c$ belonging to the percolation cluster drops with r.

For moderately long spin relaxation times $\tau_s > \tau_0$ [regime (B)], the maximum of Eq. (57) is reached at the optimal value $r = r_{\rm opt}$:

$$r_{\rm opt}(\tau_s) = \frac{a_b}{2}\ln\frac{3\tau_s}{\tau_0}, \tag{60}$$

where we neglect the contribution $\propto r^3$ in Eq. (57) in comparison with the fast exponents. The optimal side $r_{\rm opt}$ is a result of the interplay of two factors. On one hand, for very large triangles the spin generation efficiency $\Gamma_{ijk}^{(0)}$ decreases exponentially. On the other hand, for small triangles the diffusion and the drift spin currents exponentially well compensate each other [21]. In other words, the spin polarization in different directions at different sites "recombines" due to fast hopping. As a result, there is an exponentially sharp maximum for optimal triangles: $\mathcal{J}^{\rm triad} \approx \mathcal{J}_0(r_{\rm opt})$, and the exact value of γ is not very important in comparison with the strong exponential dependence $\mathcal{J}_0(r)$.

The time τ_d corresponding to start of diffusion is related to hopping on the critical distance r_c:

$$\tau_d \approx \tau_0 \exp(2r_c/a_b).$$

The larger is the spin relaxation time τ_s, the larger is the optimal triangle $r_{\rm opt}$. Provided $r_{\rm opt} < r_c$, the diffusive medium in our model does not play an essential role because the generated spin relaxes faster than τ_d. Therefore, the contribution $\mathcal{J}^{\rm med}$ can be neglected, and the total spin current $\mathcal{J} \approx \mathcal{J}^{\rm triad}$. As a result, we obtain for regime (B)

$$\mathcal{J}_y \propto \mathcal{J}_0[r_{\rm opt}(\tau_s)] \propto 1/\sqrt{\tau_s}. \tag{61}$$

In the regimes (C) and (D), the size of the optimal triangle $r_{\rm opt}(\tau_s)$ is larger than the critical distance r_c. In this case, the main contribution to $\mathcal{J}^{\rm triad}$ is given by the largest triads along the percolation cluster. At the same time, the spin polarization is partially transferred to the diffusive medium. It follows from Eq. (51) that the contribution to the spin current from the diffusive medium has the form

$$\mathcal{J}_{ijk}^{\rm med} = \tilde{S}_i^{(ijk)}F(y_i) + \tilde{S}_j^{(ijk)}F(y_j) + \tilde{S}_k^{(ijk)}F(y_k), \tag{62}$$

where

$$F(y) = \frac{1}{\tau_s\tau_d}\int_{-L/2}^{L/2} K(y', y)y'dy' \tag{63}$$

with

$$K(y', y) = \frac{\tau_s}{l_s}\frac{\mathrm{ch}\left(\frac{L-|y-y'|}{l_s}\right) + \mathrm{ch}\left(\frac{y+y'}{l_s}\right)}{2\,\mathrm{sh}\,(L/l_s)} \tag{64}$$

being the Green's function of the diffusion equation. Here, $|y| < L/2$ with L being the sample length, and $l_s = \sqrt{D\tau_s}$ is the spin diffusion length. Substitution of this expression into Eq. (63) yields

$$F(y) = \frac{1}{\tau_d}\left[y - l_s\frac{\mathrm{sh}(y/l_s)}{\mathrm{ch}(L/2l_s)}\right]. \tag{65}$$

The sizes of triangles (ikj) are much smaller than l_s in regimes (C) and (D). This allows us to relate the contribution $\mathcal{J}_{ijk}^{\rm med}$ to $\mathcal{J}_{ijk}^{\rm triad}$: $\mathcal{J}_{ijk}^{\rm med} = \tau_s\mathcal{J}_{ijk}^{\rm triad}dF/dy$, where we have taken into account Eq. (52). The contribution $\mathcal{J}^{\rm med}$ from all the triads is

$$\mathcal{J}^{\rm med} = \mathcal{J}^{\rm triad}\frac{\tau_s}{\tau_d}\left[1 - \frac{2l_s}{L}\,\mathrm{th}\left(\frac{L}{2l_s}\right)\right]. \tag{66}$$

Here, the multiplier τ_s/τ_d describes the ratio of the times spent by the spin inside the triad and outside of it. In the regime (C) one has $\tau_s \ll L^2/D$ ($l_s \ll L$), so the mesoscopic effects do not take place. In this case, the second terms in Eqs. (65) and (66) can be neglected, and $\mathcal{J}_y \approx \mathcal{J}^{\rm med}$ is independent of τ_s. However, in the regime (D) the spin separation in the sample is suppressed due to diffusion of spin polarization from one boundary of the sample to the opposite one (Fig. 3). In this regime for $l_s \gg L$ we obtain

$$\mathcal{J}_y \approx \mathcal{J}^{\rm med} \propto 1/\tau_s. \tag{67}$$

Vanishing of the spin current in the limit $\tau_s \to \infty$ has the same origin as in the two-dimensional disordered systems with spin-orbit interaction only [63].

2. Nonzero magnetic field

Now, we proceed to the analysis of the spin susceptibility as a function of an external magnetic field. This dependence is related to the factor $\cos\varphi_{ikj}$ in Eq. (49) which means that the spin separation and spin generation rates in each triad of sites oscillate as functions of B_z. Hence, one can expect the oscillations of the spin susceptibility similar to Aharonov-Bohm oscillations. Numerical calculation indeed demonstrates this effect, as shown in Fig. 4. The decay of oscillations is determined by the spread of oscillations period in optimal triads. If the spread of triad areas is much smaller than the mean area, then the period of Aharonov-Bohm oscillations in a macroscopic system is well defined. Otherwise, the oscillations are efficiently smeared.

In the regime (A) the optimal triads are the isosceles triangles with one small side $r_a \sim a_b$ (see Appendix A). The long sides of the triangle $r_{\rm side}$ can be arbitrarily large. However, we assume that these long sides participate in the percolation cluster $r_{\rm side} < r_c$. The contribution of such a triangle to the spin current $\mathcal{J}_{ijk}$ in the regime (A) is

$$\mathcal{J}_{iso} = \frac{3\hbar\alpha_{xy}\alpha_{yx}I_{\rm perc}}{16J_0\tau_0} r_{\rm side} r_a^2 \cos\theta e^{-r_a/a_b} \times \cos\left(2\pi\frac{B_z r_{\rm side} r_a}{2\Phi_0}\right). \tag{68}$$

Here, θ is an angle between the long sides of the triangle and the x axis and we have taken into account that $r_a \ll r_{\rm side}$. This contribution exponentially drops with r_a, therefore, the area of the optimal triangle can be arbitrarily small. According to Eq. (56), this expression should be averaged over different optimal triangles to obtain the magnetic-field dependence of spin susceptibility. Averaging over θ yields a factor on order of unity. The distribution of the short sides r_a is related to the probability to find a third site k participating in the percolation cluster near one of the sites i or j. The third site k should form an approximately isosceles triangle with sites i and j, $|r_{ij} - r_{jk}| \lesssim a_b$. The probability to find this site can be estimated as $n_s a_b dr_a$. Integration of Eq. (68) with this probability yields the contribution to the spin current of the isosceles triangles averaged over r_a in the form

$$\langle\mathcal{J}_{iso}\rangle_{r_a} \sim \frac{\hbar\alpha_{xy}\alpha_{yx}I_{\rm perc}n_s a_b^4 r_{\rm side}}{J_0\tau_0} \times \frac{1-3(\pi B_z a_b r_{\rm side}/\Phi_0)^2}{[1+(\pi B_z a_b r_{\rm side}/\Phi_0)^2]^3}. \tag{69}$$

The total spin current in the regime (A) is given by averaging of this expression over $r_{\rm side}$. The distribution of distances $r_{\rm side}$ between sites in the percolation cluster is not uniform. When $r_{\rm side} \ll n_s^{-1/2}$ it can be estimated as $p_A(r_{\rm side}) = p_0 r_{\rm side}$ where p_0 is a constant. This distribution reflects the fact that the probability to find a small triangle with $r_{\rm side} \ll r_c$ in the percolation cluster raises with $r_{\rm side}$. We extrapolate this distribution up to the largest possible $r_{\rm side} = r_c$. It leads to the following expression for the spin current in the regime (A):

$$f(B_z) = f(0)\frac{3}{x^3}\left[\frac{x+2x^3}{(1+x^2)^2} - \arctan x\right], \tag{70}$$

where $x = B_z r_c/(2B_0 a_b)$. The function (70) does not oscillate but it contains one change of sign.

In the regimes (B)–(D), as discussed above, the optimal triads form equilateral triangles (see also Appendix A). An exponentially sharp maximum exists in the dependence $\mathcal{J}_0(r)$ meaning that the dominant contribution to SHE comes from the triangles with the same area. With account for the Aharonov-Bohm phase

$$\cos\left(\frac{\pi B_z r^2\sqrt{3}}{2\Phi_0}\right), \tag{71}$$

we evaluate the integral (58) by the stationary-phase method and obtain the magnetic-field dependence of the spin susceptibility in the form

$$f(B_z) = f(0)\cos\left(\frac{B_z}{B_{\rm opt}}\right)\exp\left(-\frac{2B_z^2}{B_{\rm opt}B_0}\right). \tag{72}$$

Here, the period of the oscillations is determined by the area of the optimal triangle:

$$B_{\rm opt} = \frac{4\hbar c}{\sqrt{3}|e|r_{\rm opt}^2}, \tag{73}$$

and the rate of oscillations decay is related to the decrease of the triad contribution to the spin current when its size deviates from the optimal one. Qualitatively, the number of oscillations is of the order of $\sqrt{B_0/B_{\rm opt}}$.

IV. DISCUSSION

The results of the previous section indicate that the dependence of the spin susceptibility on τ_s as well as its oscillations as a function of the magnetic field are closely related to the spin transport in strongly disordered sample.

The sum of two contributions, Eqs. (58) and (66), describe the total spin current in the framework of the percolation analysis at zero magnetic field for any τ_s. The corresponding calculation of the spin susceptibility $f(\tau_s, n_s)$ is shown by the white line in Fig. 2. Reasonably good agreement of the percolation analysis with the results of numerical calculations is evident for all the regimes. Moreover, the analytical dependencies $1/\sqrt{\tau_s}$ for regime (B) [Eq. (61)] and $1/\tau_s$ for regime (D) [Eq. (67)] as well as constants for regimes (A) and (C) describe the numerical simulations with high accuracy. The contributions to the spin current from triads and from the diffusive media are shown in Fig. 2 by yellow and green lines, respectively. Figure 2 demonstrates that the triads' contribution dominates in the regimes (A) and (B). In contrast, triads serve only as sources of the spin current in the regimes (C) and (D) where the diffusive media contribution is the largest.

We note, however, that the diffusion coefficient $D = 0.5\times10^{-8}a_b^2/\tau_0$ used in the analytical calculation in Fig. 2 is different from the charge diffusion coefficient, obtained from the numerical simulation of system conductivity $5.6\times10^{-5}a_b^2/\tau_0$, and from the estimation $L_{\rm cor}^2/\tau_d \approx 2.9\times$

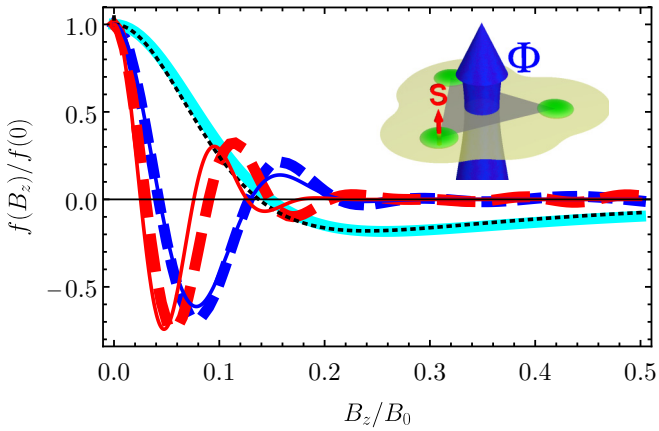

FIG. 5. Magnetic-field dependencies of the normalized spin susceptibility for $\tau_s/\tau_0 = 10^{-3}$ (cyan curve), 3×10^7 (blue dashed curve), and 4×10^{14} (red dashed curve). Parameters of the calculation are the same as in Fig. 2. The numerical results for the susceptibility are compared with Eq. (70) (dashed black curve) and with Eq. (72) (solid blue and red curves). The inset illustrates the magnetic flux through a triad of localization sites responsible for Aharonov-Bohm-type oscillations.

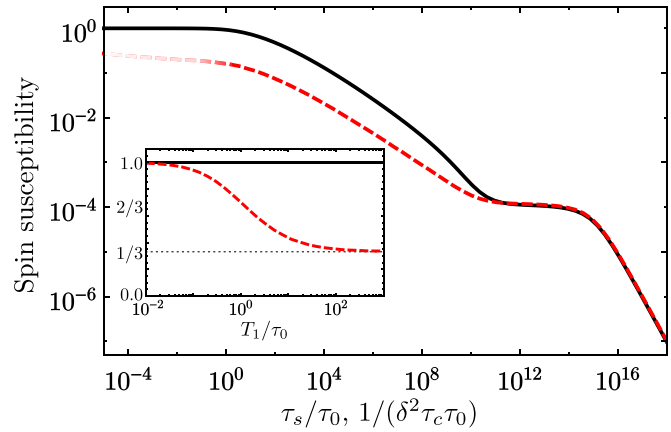

FIG. 6. The dependencies $f(\tau_s/\tau_0)$ (black solid curve) and $f[1/(\delta^2\tau_c\tau_0)]$ (red dashed curve) calculated in the models with a single spin relaxation time [Eq. (56)] and in the model of nuclei-induced spin relaxation, Appendix B, respectively. The parameters of the calculation are the same, as in Fig. 2, and $T_1 = \infty$. The inset shows the dependence of $f(T_1)$ in the regime (A) ($T_1\delta = 10^4$), where $f = 1$ in the model with a single spin relaxation time.

$10^{-6}a_b^2/\tau_0$. This is most probably an artifact of our oversimplified model.

Figure 5 demonstrates the magnetic-field dependence of the spin susceptibility for the regimes (A)–(D). The colors of the curves correspond to the background colors in Fig. 2. We note that the magenta curve in the figure is absent because it coincides with the red one. The dependence (70) is shown by the black dashed curve in Fig. 5. The very good agreement between Eq. (70) and numerical simulation results in the regime (A) is clearly seen. The numerical results for the regimes (B)–(D) agree qualitatively with Eq. (72) as shown by solid blue and red curves in Fig. 5. Moreover, the analytical expression (73) for the oscillation period is in quantitative agreement with numerical results in the regime (B). In the regimes (C) and (D), the agreement is slightly less perfect: for $\tau_s/\tau_0 = 4 \times 10^{14}$ the numerical result for the period exceeds the analytical estimate (73) by ∼18%.

Because of suppression of spin polarization with increase of magnetic field, we focused mainly on the even in magnetic field effects which are described by the spin susceptibility $f(n_s, \tau_s)$. The odd in B_z kinetic coefficients contain energy differences between initial and intermediate states [Eq. (22a)]. Therefore, they can not be analyzed neglecting energy disorder, as it is done in Sec. III. We note, however, that these terms can vanish due to this averaging, which deserves a separate study.

We note that the definitions of macroscopic susceptibilities [Eqs. (41)–(44)] are valid for the particular form of spin-orbit interaction [Eq. (2)], which is realized in zinc-blende heterostructures grown along [001] direction. Nevertheless, the presented results can be applied to a wider class of systems, where one can choose the reference frame in the spin space formally coinciding with Eq. (2). This can be done, in particular, for asymmetric structures grown along the [110] direction. Moreover, despite all three effects in (001) heterostructures are related with the in-plane spin components, in (110) quantum wells the electric current orients the spin component normal to the 2D plane. If the (110) system is structure asymmetric, then its point symmetry group is C_s with a reflection in the (yz) plane being only one nontrivial symmetry element. Here, $z \parallel [110]$ is the normal direction, and $x \parallel [\bar{1}10]$, $y \parallel [001]$ are the in-plane axes [25]. The symmetry analysis shows that the following even in B_z components are nonzero:

$$\sigma^{xy,yx}_{\mathrm{CISP,SGE,SHE}}, \qquad \sigma^{zx}_{\mathrm{CISP}}, \qquad \sigma^{xz}_{\mathrm{SGE}}, \tag{74}$$

as well as the following odd in B_z ones:

$$\sigma^{xx,yy}_{\mathrm{CISP,SGE,SHE}}, \qquad \sigma^{zy}_{\mathrm{CISP}}, \qquad \sigma^{yz}_{\mathrm{SGE}}. \tag{75}$$

Due to low symmetry, all these components are linearly independent.

In this paper, we neglected Zeeman effect, which does not affect the spin current. However, external magnetic field can significantly suppress the in-plane spin polarization due to Hanle effect as $1/[1 + (g\mu_B B_z \tau_s/\hbar)^2]$ with g being effective electron g factor and μ_B being Bohr magneton. Interestingly, in the structures of crystallographic orientations other than (110), the Hanle effect can manifest itself as only partial suppression of spin polarization. Detailed analysis of these effects is beyond the scope of this paper.

For localized charge carriers, the main source of spin relaxation is the hyperfine interaction with the host lattice nuclei [27,28,64–68]. Since the spin relaxation time of nuclei is very long, the electron spin relaxation is non-Markovian [66]. Generally, the spin relaxation can not be described by a single time τ_s, as it is assumed in our simplified model. Therefore, we also study the generalized susceptibility in a more realistic model of nuclei-induced spin relaxation. Details of the model are given in Appendix B. The result is shown by a red dashed line in Fig. 6 along with the dependence $f(\tau_s/\tau_0)$ calculated in the simplified model after Eq. (56) (black solid line). The nuclei-induced spin relaxation rate is determined by the

typical value of the fluctuation of the Overhauser field at the localization site δ [Eq. (B4)].

Figure 6 demonstrates that the dependencies of f on τ_s/τ_0 in a simple model and on $1/(\delta^2\tau_c\tau_0)$, where $\tau_c = \tau_0 e^{2r_c/a_b}$ are similar: they both consist of the four distinct regimes. Therefore, we conclude that our main model qualitatively describes the spin-related phenomena even in the case of nuclei-induced spin relaxation. The two models coincide in the regimes (C) and (D) because in this case the electron spins make many hops before relaxation, and one can introduce an effective spin relaxation time (see, however, Refs. [67,68]). In the regime (B), the dominant contribution to the generalized spin susceptibility is given by equilateral triads, as discussed in Sec. III B 1. The spin relaxation in the triads is determined by the fluctuations of the Overhauser field at these three sites, and to obtain the value of f one should average the diffusive spin current over the distribution of the nuclear fields. Figure 6 shows that the total spin current in this case is smaller than in the model with a single spin relaxation time τ_s (details of calculations are described in Appendix B). This explains the quantitative difference between the two models in the regime (B). With an increase of hyperfine interaction strength [in the regime (A)] the generalized spin susceptibility saturates at a value smaller than 1. This is related with the fact that, on average, only $\frac{2}{3}$ of the generated spin polarization decays due to static nuclear spin fluctuations at a given site [27]. Therefore, we introduce an additional phenomenological slow spin relaxation time T_1 unrelated with the hyperfine interaction which leads to complete relaxation of spin polarization in the limit of very long hopping time. In the regime (A), the generalized spin susceptibility depends on T_1 at $T_1 \lesssim \tau_0$. The dependence $f(T_1/\tau_0)$ is shown in the inset in Fig. 6. One can see, that in the limit $T_1 \ll \tau_0$, the generalized spin susceptibility equals to 1 and agrees with the result of the single spin relaxation time model.

V. CONCLUSION

Based on the derived kinetic equations describing the coupled spin-charge dynamics, we have identified four regimes of hopping spin transport where SHE, CISP, and SGE have different behavior. The numerical simulation shows the map of the spin distribution in the sample in all four regimes. The spin susceptibility is shown to be governed by the ratio of the spin relaxation and hopping times. The percolation analysis being in a very good agreement with the numerical simulations demonstrates how the contributions to the spin effects from each triad in the percolation cluster average over disorder realizations. Application of the perpendicular magnetic field results in damped oscillations of the spin susceptibility where the number of sign changes is also determined by the spin relaxation time.

ACKNOWLEDGMENTS

The financial support from the Foundation for advancement of theoretical physics and mathematics "BASIS" is gratefully acknowledged. The work of D.S.S. and L.E.G. was supported by Russian Science Foundation (Project No. 17-12-01265).

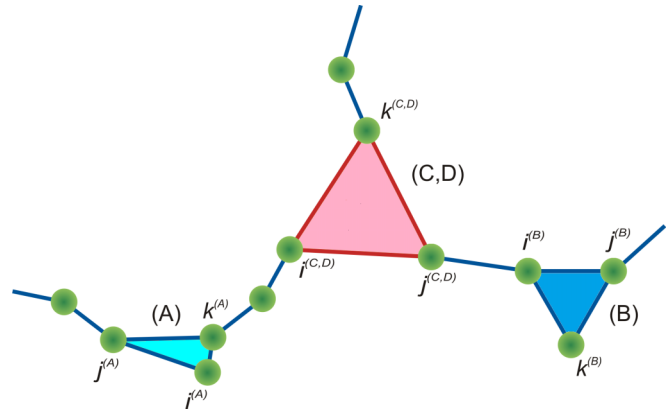

FIG. 7. A part of the percolation cluster. The noncritical resistors participating in the cluster are shown with blue color. The critical resistors are shown with red color. The area of the optimal triangles in different regimes is filled in accordance with the background colors in Fig. 2.

APPENDIX A: OPTIMAL TRIADS

In our percolation analysis we discussed that the contributions of different triads of sites to SHE have an exponentially broad distribution. The effect is dominated by the optimal triads of sites ikj that are defined by optimal geometry of the corresponding triangle (ikj). However, this geometry is different in different regimes. Here, we discuss in details the optimal geometry in all the regimes (A)–(D).

In the regime (A) all the hopping terms can be neglected in Eqs. (50). It allows to write the solution explicitly:

$$\widetilde{S}_i^{(ikj)} = \tau_s' I_{kj}\tau_{kj}\Gamma_{ijk}^{(0)} \propto I_{kj}\exp\left(\frac{r_{kj}-r_{ij}-r_{ik}}{a_b}\right). \quad \text{(A1)}$$

The similar expressions can be derived for $\widetilde{S}_j^{(ikj)}$ and $\widetilde{S}_k^{(ikj)}$. The exponential part of Eq. (A1) disappears in the isosceles triangle with

$$r_{ij} = r_{kj}, \quad r_{ik} \sim a_b. \quad \text{(A2)}$$

The long sides r_{ij} and r_{kj} are assumed to belong to the percolation cluster (see a cyan triangle in Fig. 7). When the geometry of the triangle deviates from the discussed one, $\widetilde{S}_j^{(ikj)}$ exponentially decreases. It is clear from Eq. (A1) that it decreases with increasing r_{ik} as $\exp(-r_{ik}/a_b)$. When the triangle ikj deviates from Eq. (A2), the generated spin decreases due to the redistribution of the currents. Let the side r_{kj} be larger than r_{ij}. The current I_{kj} in this case can be estimated as $I_{kj} = I_{\rm perc}\exp[-2(r_{kj}-r_{ij})/a_b]$. It leads to the additional exponentially small term $\exp(-|r_{kj}-r_{ij}|/a_b)$ in the expression for the generated spin. When $r_{ij} > r_{kj}$ the current I_{kj} is equal to $I_{\rm perc}$, but the term $\exp(-|r_{kj}-r_{ij}|/a_b)$ appears in Eq. (A1) directly.

The optimal triangle in the regime (B) is the equilateral triangle with a side $r_{\rm opt}$ given by Eq. (60) (see a blue triangle in Fig. 7). The triangle should participate in the percolation cluster. As mentioned in the main text, the discussed geometry is actually the optimal one. To prove this, we consider the triangle with $y_i = y_j = 0$. The side ij of the triangle is assumed to be included into the percolation cluster. Its

contribution to spin current is directly related to $\widetilde{S}_k^{(ikj)}$ as $\mathcal{J}_{ikj}^{(\mathrm{triad})} = \widetilde{S}_k^{(ikj)} y_k/\tau_s$. We remind that in the regime (B), $\tau_s' \approx \tau_s \ll \tau_d$, and the contribution $\mathcal{J}_{ikj}^{(\mathrm{med})}$ can be neglected.

We start with the comparison of the contributions to the spin current of equilateral triangles with different length r of the side. In this case, $\tau_{ik} = \tau_{ij} = \tau_{jk} = \tau_0 e^{2r/a_b}$, $\tau_{ikj}' = \tau_0' e^{3r/a_b}$, $\tau_0' = (4/3\hbar) J_0 \tau_0^2$. The system of equations (50) in this case can be analytically solved:

$$\widetilde{S}_k^{(ikj)} = \frac{2}{3} I_{\mathrm{perc}} \frac{\tau_s \tau_0}{\tau_0'} \frac{\alpha_{xy}\alpha_{yx} A_{ijk}^z e^{r/a_b}}{e^{2r/a_b} + 3\tau_s/\tau_0}. \tag{A3}$$

In our analysis we neglect the power-law dependence $A_{ijk}^z(r)$ in comparison to exponential dependence $\sim e^{r/a_b}$ of the right-hand side of Eq. (A3). This expression has a maximum at $r = r_{\mathrm{opt}}$:

$$\widetilde{S}_k^{(\mathrm{opt})} = \frac{\alpha_{xy}\alpha_{yx} A_{\mathrm{opt}} I_{\mathrm{perc}} \tau_0^{3/2} \tau_s^{1/2}}{3\sqrt{3}\tau_0'}, \tag{A4}$$

where $A_{\mathrm{opt}} = (\sqrt{3}/4) r_{\mathrm{opt}}^2$.

Now, we should compare a contribution of nonequilateral triangles with expression (A4). In this procedure we consider $r_{ij} = r_{\mathrm{opt}}$ and displace the site k from its position corresponding to the equilateral triangle. If we move the site along the x axis, one of the sides r_{ik} and r_{jk} becomes larger than another. Let us consider $r_{ik} < r_{jk}$. In the limit $n_s a_b^2 \ll 1$, it means that $\tau_{ik} \ll \tau_{ij} \ll \tau_{jk}$. However, at least for relatively small displacements we can still consider $\tau_{ikj}' = \tau_0' e^{3r_{\mathrm{opt}}/a_b}$. Also, the spin relaxation rate is comparable with τ_{ij} because r_{ij} is still equal to r_{opt}: $\tau_s = \tau_{ij}/3$. In this case, we can neglect the term τ_s/τ_{kj} in the equation for S_j and disregard spin diffusion between sites j and k. Also, the spin generation at the site j is exponentially smaller than at sites i and k and can be neglected. It leads to the relation between the polarizations on sites i and j: $\widetilde{S}_j^{(ikj)} = \widetilde{S}_i^{(ikj)}/4$. With Eq. (52) it allows us to give an explicit expression for $\widetilde{S}_k^{(ikj)}$:

$$\begin{aligned}\widetilde{S}_k^{(ikj)} &= \frac{5}{3} \frac{I_{\mathrm{perc}} \tau_s \tau_{ik} \alpha_{xy}\alpha_{yx} A_{\mathrm{opt}} \tau_{ik}}{\tau_0' e^{3r_{opt/a}}} \\ &\sim \widetilde{S}_k^{(\mathrm{opt})} e^{2(r_{ik}-r_{ij})/a_b} \ll \widetilde{S}_k^{(\mathrm{opt})}.\end{aligned} \tag{A5}$$

Now, we consider the displacement of the site k along the y axis. For this displacement the triangle ikj stays isosceles. Therefore, the relation of the spins $\widetilde{S}_i^{(ikj)}$, $\widetilde{S}_j^{(ikj)}$, and $\widetilde{S}_k^{(ikj)}$ is the same as in the case of equilateral triangle $\widetilde{S}_i^{(ikj)} = \widetilde{S}_j^{(ikj)} = -\widetilde{S}_k^{(ikj)}/2$. It leads to the explicit expression for $\widetilde{S}_k^{(ikj)}$:

$$\begin{aligned}\widetilde{S}_k^{(ikj)} &= I_{ij}\tau_{ij} \frac{\alpha_{xy}\alpha_{yx} A_{ikj}^z}{\tau_0'} \frac{\tau_s \tau_{\mathrm{side}}}{\tau_{\mathrm{side}} + 3\tau_s} \\ &\times \exp\left(-\frac{r_{ij} + 2r_{\mathrm{side}}}{a_b}\right).\end{aligned} \tag{A6}$$

Here, $r_{ik} = r_{jk} = r_{\mathrm{side}}$ and $\tau_{\mathrm{side}} = \tau_0 \exp(2r_{\mathrm{side}}/a_b)$. When $r_{\mathrm{side}} = r_{ij}$, the current $I_{ij} = 2I_{\mathrm{perc}}/3$, and Eq. (A6) is reduced to Eq. (A3). When r_{side} is larger than r_{ij}, the last term in Eq. (A6) exponentially decreases, leading to the exponentially small spin polarization $\widetilde{S}_k^{(ikj)}$. When $r_{\mathrm{side}} < r_{ij}$ the current I_{ij} becomes small, $I_{ij} \sim I_{\mathrm{perc}} \exp[-2(r_{ij} - r_{\mathrm{side}})/a_b]$, because the resistor R_{ij} is shunted by the resistors R_{ik} and R_{kj}. It again leads to the exponentially small spin generation $\widetilde{S}_k^{(ikj)}$.

The above arguments prove that, in the regime (B), the dominant contribution to the spin Hall effect comes from the equilateral triangles with sides r_{opt}. r_{opt} increases with τ_s and becomes larger than r_c at $\tau_s \gg \tau_0 \exp(2r_c/a_b)$. This spin relaxation time corresponds to the transition from regime (B) to regime (C). In the above analysis we assumed that the triangle ikj is included into the percolation cluster. It is not possible when $r_{ij} > r_c$, leading to the upper boundary for the side of the optimal triangle. Therefore, in the regimes (C) and (D) the dominant triangles have sides $\sim r_c$.

The spin generation in the regimes (C) and (D) is controlled not only by the processes inside the triangle ikj, but also by the transition of the spin to the surrounding medium. It leads to the additional restrictions for the position of the triangle ikj. All the three sites of the triangle should be parts of the percolation cluster, otherwise the effective transition of spin from the triangle to the medium is impossible. However, they should be included in different branches of the cluster, otherwise the resistors of the triangle will be shunted by the noncritical resistors of the cluster. The optimal triangle in regimes (C) and (D) is shown in Fig. 7. It lies at the intersection of three branches of the percolation cluster.

In the limit $\tau_s \to \infty$, our theory of SHE can be mapped on the theory of the ordinary hopping Hall effect. The optimal triangles for the Hall effect are discussed in Ref. [55]. Our predictions for the optimal triangles in regimes (C) and (D) agree with this work.

APPENDIX B: HYPERFINE-INTERACTION-INDUCED SPIN RELAXATION

The results of the main text were obtained in the framework of the simplified model where spin relaxation is described by a single time τ_s. When the dominant spin relaxation mechanism is the hyperfine interaction with the host lattice nuclei, the physics of the spin relaxation is more complicated. Although the detailed analysis of the interplay of the realistic spin relaxation and spin-orbit interaction is out of the framework of this study, we show here that our main result, the existence of the four fundamental regimes (A)–(D), is relevant for the hyperfine-interaction-induced spin relaxation mechanism.

In the regimes (C) and (D), electrons make many hops before the spin relaxes. In this case, the spin density decays in time exponentially, and the spin relaxation time τ_s can be introduced. Our results for these regimes are valid for the hyperfine-interaction-induced spin relaxation mechanism. However, it should be noted that the spin relaxation time depends on both the spin precession frequency and the hopping time.

In contrast, in the regimes (A) and (B), all important processes take place inside the triads, and the Overhauser field induced spin dynamics cannot be reduced to a single spin relaxation time. However, the system of rate equations for the electron spin with the spin precession can be readily solved numerically. The results then are averaged over the hyperfine

fields and the triads. We make these numerical calculations in the following subsections. The provided results show that the four above-discussed regimes are relevant when the realistic spin dynamics in the hyperfine fields is considered despite that the physics is different, especially in the regime (B).

1. Regimes (B), (C), and (D)

In the regimes (B), (C), and (D) we restrict ourselves with the equilateral triangles that are known to control the effects in the single τ_s model. The spin dynamics inside the triangle can be described by the equations [cf. Eqs. (50)]

$$\widetilde{\boldsymbol{S}}_i^{(ijk)} \times \boldsymbol{\omega}_i + \frac{\widetilde{\boldsymbol{S}}_i^{(ijk)}}{\tau_d} + \frac{2\widetilde{\boldsymbol{S}}_i^{(ijk)} - \widetilde{\boldsymbol{S}}_j^{(ijk)} - \widetilde{\boldsymbol{S}}_k^{(ijk)}}{\tau} = \frac{1}{3} I_{\rm perc}\tau\Gamma_{ijk}^{(0)}\boldsymbol{e}_z, \tag{B1}$$

$$\widetilde{\boldsymbol{S}}_j^{(ijk)} \times \boldsymbol{\omega}_j + \frac{\widetilde{\boldsymbol{S}}_j^{(ijk)}}{\tau_d} + \frac{2\widetilde{\boldsymbol{S}}_j^{(ijk)} - \widetilde{\boldsymbol{S}}_i^{(ijk)} - \widetilde{\boldsymbol{S}}_k^{(ijk)}}{\tau} = \frac{1}{3} I_{\rm perc}\tau\Gamma_{ijk}^{(0)}\boldsymbol{e}_z, \tag{B2}$$

$$\widetilde{\boldsymbol{S}}_k^{(ijk)} \times \boldsymbol{\omega}_k + \frac{\widetilde{\boldsymbol{S}}_k^{(ijk)}}{\tau_d} + \frac{2\widetilde{\boldsymbol{S}}_k^{(ijk)} - \widetilde{\boldsymbol{S}}_i^{(ijk)} - \widetilde{\boldsymbol{S}}_j^{(ijk)}}{\tau} = -\frac{2}{3} I_{\rm perc}\tau\Gamma_{ijk}^{(0)}\boldsymbol{e}_z. \tag{B3}$$

Here, $\widetilde{\boldsymbol{S}}_i^{(ijk)}$ stands for the vector of the spin polarization at the site i of the triangle (ijk), $\tau = \tau_{ij} = \tau_{ik} = \tau_{jk}$ is the hopping time between the sites of the triangle, τ_d is the time of the spin transition to the medium, and $\boldsymbol{\omega}_i$, $\boldsymbol{\omega}_j$, $\boldsymbol{\omega}_k$ are the frequencies of the spin precession at the sites of the triangle. The vectors $\boldsymbol{\omega}_{i,j,k}$ are assumed to be independent and have the Gaussian distribution characterized by a parameter δ:

$$\mathcal{F}(\boldsymbol{\omega}) = \frac{1}{(\sqrt{\pi}\delta)^3}\exp\left(-\omega^2/\delta^2\right). \tag{B4}$$

The triangle is assumed to be connected to the percolation cluster as it is shown in Fig. 7. This defines the right-hand side of the equations. The spin generation rate is multiplied by $\boldsymbol{e}_z$ to reflect the fact that the spin is generated along the z axis in the lowest (second) order in the spin-orbit interaction. We assume that only the z component of spin exists in the medium. Its dynamics is described by Eq. (51) of the main text where the spin relaxation time in the medium is introduced according to

$$\tau_s = 1/(\delta^2\tau_c), \tag{B5}$$

where $\tau_c = \tau_0 e^{2r_c/a_b}$ is the characteristic time of the spin diffusion.

In Fig. 6, we compare the results of the above-discussed model with the results of the single spin relaxation time model. In the regimes (C) and (D), the results coincide. In the regime (B), the results are similar: both models demonstrate a decrease of the spin susceptibility with the increase of the spin relaxation rate.

2. Regime (A)

When $\delta\tau_0 \gg 1$, the spin precession is fast as compared with the hopping rate and the system is in the regime (A). Although the spin can not relax completely due to the regular precession in the hyperfine fields (only $\frac{2}{3}$ of the spin polarization decays on average [27]), the partial relaxation breaks the detailed balance between the drift and diffusion spin currents. As a result, in the limit $\delta\tau_0 \gg 1$ the spin susceptibility tends to a constant of the order of unity.

In the single spin relaxation time model, the spin current in the regime (A) is associated only with the spin generation (drift current). The dominant role is played by the isosceles triangles with one short side $r_{ik} \sim a$ (Fig. 7). Spin generation in the other triangles is exponentially smaller. Let us reconsider these triangles with the model of realistic spin dynamics (spin precession in the local fields).

The spin generation in the triangle with $r_{ik} \sim a$, $r_{ij}, r_{jk} \gg a$ is most efficient at the sites i and k. The spin polarization at the site j can be neglected. This leads to the following system of equations:

$$\widetilde{\boldsymbol{S}}_i^{(ijk)} \times \boldsymbol{\omega}_i - \frac{\widetilde{\boldsymbol{S}}_k^{(ijk)} - \widetilde{\boldsymbol{S}}_i^{(ijk)}}{\tau_{ik}} + \frac{\widetilde{\boldsymbol{S}}_i^{(ijk)}}{T_1} = \boldsymbol{g}_{ijk},$$

$$\widetilde{\boldsymbol{S}}_k^{(ijk)} \times \boldsymbol{\omega}_k - \frac{\widetilde{\boldsymbol{S}}_i^{(ijk)} - \widetilde{\boldsymbol{S}}_k^{(ijk)}}{\tau_{ik}} + \frac{\widetilde{\boldsymbol{S}}_k^{(ijk)}}{T_1} = -\boldsymbol{g}_{ijk}, \tag{B6}$$

where $\boldsymbol{g}_{ijk} \parallel z$, $g_{ijk} = I_{\rm perc}\tau_{ij}\Gamma_{ijk}^{(0)}/2$. Here, we introduced a long phenomenological spin relaxation time T_1 unrelated with the hyperfine interaction in order to describe the relaxation of spin component parallel to $\boldsymbol{\omega}_{i,k}$ without hopping. Microscopically, it can be caused by the two-phonon processes [69]. The z component of the spin current is expressed according to Eqs. (26) and (38) of the main text. We note that the spin current is equal to zero when $\boldsymbol{\omega}_j = \boldsymbol{\omega}_k = 0$ and $T_1 \to \infty$.

We solve these equations in the limit $|\boldsymbol{\omega}_{i,k}|\tau_0 \gg 1$. In this case, it is useful to divide $\widetilde{\boldsymbol{S}}_{i,k}^{(ijk)}$ into the components oriented along the local field $\boldsymbol{\omega}_{i,k}$ and perpendicular to it. The perpendicular component experiences fast precession. Its average value is proportional to $1/|\boldsymbol{\omega}_{i,k}|$, so it can be neglected. It allows us to solve Eqs. (B6) and obtain the following result in the limit of fast spin precession and $T_1 \to \infty$:

$$f_{ijk} = 1 - \frac{\cos^2\theta_{iz} - 2\cos\theta_{iz}\cos\theta_{ik}\cos\theta_{kz} + \cos^2\theta_{kz}}{1 - \cos^2\theta_{ik}}. \tag{B7}$$

Here, f_{ijk} is the spin susceptibility for the given orientations of the vectors $\boldsymbol{\omega}_{i,k}$ with $\theta_{iz,kz}$ being the angles between $\boldsymbol{\omega}_{i,k}$ and the z axis, and θ_{ik} being the angle between $\boldsymbol{\omega}_i$ and $\boldsymbol{\omega}_k$. Averaging f_{ijk} over these angles yields

$$f(|\boldsymbol{\omega}_{i,k}| \to \infty) = 1/3. \tag{B8}$$

The results of calculations for the regime (A) are shown in the inset in Fig. 6. A transition from $f = 1$ to $\frac{1}{3}$ given by Eq. (B8) takes place when T_1 becomes longer than τ_0.

[1] *Spin Physics in Semiconductors*, edited by M. I. Dyakonov (Springer, Berlin, 2016).

[2] M. I. Dyakonov and V. I. Perel', Possibility of orienting electron spins with current, Pisma Zh. Eksp. Teor. Fiz. **13**, 657 (1971) [Sov. Phys. JETP Lett. **13**, 467 (1971)].

[3] M. I. Dyakonov and V. I. Perel', Current induced spin orientation of electrons in semiconductors, Phys. Lett. A **35**, 459 (1971).

[4] Y. K. Kato, R. C. Myers, A. C. Gossard, and D. D. Awschalom, Observation of the spin Hall effect in semiconductors, Science **306**, 1910 (2004).

[5] J. Schliemann, Spin Hall effect, Int. J. Mod. Phys. B **20**, 1015 (2006).

[6] V. K. Kalevich, V. L. Korenev, and I. A. Merkulov, Nonequilibrium spin and spin flux in quantum films of GaAs-type semiconductors, Solid State Commun. **91**, 559 (1994).

[7] E. Saitoh, M. Ueda, H. Miyajima, and G. Tatara, Conversion of spin current into charge current at room temperature: Inverse spin-Hall effect, Appl. Phys. Lett. **88**, 182509 (2006).

[8] T. Kimura, Y. Otani, T. Sato, S. Takahashi, and S. Maekawa, Room-Temperature Reversible Spin Hall Effect, Phys. Rev. Lett. **98**, 156601 (2007).

[9] E. L. Ivchenko and G. E. Pikus, New photogalvanic effect in gyrotropic crystals, Pisma Zh. Eksp. Teor. Fiz. **27**, 640 (1978) [Sov. Phys. JETP Lett. **27**, 604 (1978)].

[10] L. E. Vorob'ev, E. L. Ivchenko, G. E. Pikus, I. I. Farbshtein, V. A. Shalygin, and A. V. Shturbin, Optical activity in tellurium induced by a current, Pisma Zh. Eksp. Teor. Fiz. **29**, 485 (1979) [Sov. Phys. JETP Lett. **29**, 441 (1979)].

[11] F. T. Vasko and N. A. Prima, Spin splitting of spectrum of 2-dimensional electrons, Sov. Phys. Solid State **21**, 994 (1979).

[12] L. S. Levitov, Yu. V. Nazarov, and G. M. Eliashberg, Magnetoelectric effects in conductors with mirror isomer symmetry, Zh. Eksp. Teor. Fiz. **88**, 229 (1979) [Sov. Phys. JETP **61**, 133 (1985)].

[13] A. G. Aronov and Yu. B. Lyanda-Geller, Nuclear electric resonance and orientation of carrier spins by an electric field, Pisma Zh. Eksp. Teor. Fiz. **50**, 398 (1989) [Sov. Phys. JETP Lett. **50**, 431 (1989)].

[14] V. M. Edelstein, Spin polarization of conduction electrons induced by electric current in two-dimensional asymmetric electron systems, Solid State Commun. **73**, 233 (1990).

[15] A. G. Aronov, Yu. B. Lyanda-Geller, and G. E. Pikus, Spin polarization of electrons by an electric current, Zh. Eksp. Teor. Fiz. **100**, 973 (1991) [Sov. Phys. JETP **73**, 537 (1991)].

[16] E. L. Ivchenko and S. D. Ganichev, in *Spin Photogalvanics*, edited by M. I. Dyakonov (Springer, Berlin, 2016).

[17] A. Yu. Silov, P. A. Blajnov, J. H. Wolter, R. Hey, K. H. Ploog, and N. S. Averkiev, Current-induced spin polarization at a single heterojunction, Appl. Phys. Lett. **85**, 5929 (2004).

[18] S. D. Ganichev, S. N. Danilov, P. Schneider, V. V. Bel'kov, L. E. Golub, W. Wegscheider, D. Weiss, and W. Prettl, Electric current-induced spin orientation in quantum well structures, J. Magn. Magn. Mater. **300**, 127 (2006).

[19] Y. K. Kato, R. C. Myers, A. C. Gossard, and D. D. Awschalom, Current-Induced Spin Polarization in Strained Semiconductors, Phys. Rev. Lett. **93**, 176601 (2004).

[20] S. D. Ganichev, M. Trushin, and J. Schliemann, in *Spin Orientation by Electric Current in Handbook of Spin Transport and Magnetism*, edited by E. Y. Tsymbal and I. Zutic (CRC Press, Boca Raton, FL, 2016).

[21] D. S. Smirnov and L. E. Golub, Electrical Spin Orientation, Spin-Galvanic, and Spin-Hall Effects in Disordered Two-Dimensional Systems, Phys. Rev. Lett. **118**, 116801 (2017).

[22] F. J. Ohkawa and Y. Uemura, Quantized surface states of a narrow-gap semiconductor, J. Phys. Soc. Jpn. **37**, 1325 (1974).

[23] F. T. Vasko, Spin splitting of spectrum of two-dimentional electrons, induced by surface potential, Pisma Zh. Eksp. Teor. Fiz. **30**, 574 (1979) [Sov. Phys. JETP Lett. **30**, 541 (1979)].

[24] M. I. Dyakonov and V. Yu. Kachorovskii, Spin relaxation of two-dimensional electrons in noncentrosymmetric semiconductors, Sov. Phys. Semicond. **20**, 110 (1986).

[25] S. D. Ganichev and L. E. Golub, Interplay of Rashba/Dresselhaus spin splittings probed by photogalvanic spectroscopy – a review, Phys. Status Solidi B **251**, 1801 (2014).

[26] K. V. Kavokin, Spin relaxation of localized electrons in n-type semiconductors, Semicond. Sci. Technol. **23**, 114009 (2008).

[27] I. A. Merkulov, Al. L. Efros, and M. Rosen, Electron spin relaxation by nuclei in semiconductor quantum dots, Phys. Rev. B **65**, 205309 (2002).

[28] A. V. Khaetskii, D. Loss, and L. Glazman, Electron Spin Decoherence in Quantum Dots due to Interaction with Nuclei, Phys. Rev. Lett. **88**, 186802 (2002).

[29] O. Gywat, H. J. Krenner, and J. Berezovsky, *Spins in Optically Active Quantum Dots: Concepts and Methods* (Wiley, Hoboken, NJ, 2009).

[30] M. M. Glazov, Coherent spin dynamics of electrons and excitons in nanostructures (a review), Phys. Solid State **54**, 1 (2012).

[31] R. J. Warburton, Single spins in self-assembled quantum dots, Nat. Mater. **12**, 483 (2013).

[32] J. M. Kikkawa and D. D. Awschalom, Resonant Spin Amplification in *n*-Type GaAs, Phys. Rev. Lett. **80**, 4313 (1998).

[33] B. Beschoten, Spin coherence in semiconductors, in *Magnetism goes Nano, 36th Spring School 2005, Schriften des Forschungzentrums Julich, Matter and Materials, Vol. 26*, edited by T. Bruckel, S. Blugel, and C. M. Schneider (Forschungszentrum Jülich, Jülich, 2005).

[34] A. Greilich, D. R. Yakovlev, A. Shabaev, Al. L. Efros, I. A. Yugova, R. Oulton, V. Stavarache, D. Reuter, A. Wieck, and M. Bayer, Mode locking of electron spin coherences in singly charged quantum dots, Science **313**, 341 (2006).

[35] I. A. Yugova, M. M. Glazov, E. L. Ivchenko, and Al. L. Efros, Pump-probe Faraday rotation and ellipticity in an ensemble of singly charged quantum dots, Phys. Rev. B **80**, 104436 (2009).

[36] I. A. Yugova, A. A. Sokolova, D. R. Yakovlev, A. Greilich, D. Reuter, A. D. Wieck, and M. Bayer, Long-Term Hole Spin Memory in the Resonantly Amplified Spin Coherence of InGaAs/GaAs Quantum Well Electrons, Phys. Rev. Lett. **102**, 167402 (2009).

[37] L. V. Fokina, I. A. Yugova, D. R. Yakovlev, M. M. Glazov, I. A. Akimov, A. Greilich, D. Reuter, A. D. Wieck, and M. Bayer, Spin dynamics of electrons and holes in InGaAs/GaAs quantum wells at millikelvin temperatures, Phys. Rev. B **81**, 195304 (2010).

[38] I. A. Yugova, M. M. Glazov, D. R. Yakovlev, A. A. Sokolova, and M. Bayer, Coherent spin dynamics of electrons and holes in semiconductor quantum wells and quantum dots under

periodical optical excitation: Resonant spin amplification versus spin mode locking, Phys. Rev. B **85**, 125304 (2012).

[39] A. Greilich, A. Shabaev, D. R. Yakovlev, Al. L. Efros, I. A. Yugova, D. Reuter, A. D. Wieck, and M. Bayer, Nuclei-induced frequency focusing of electron spin coherence, Science **317**, 1896 (2007).

[40] M. M. Glazov, I. A. Yugova, S. Spatzek, A. Schwan, S. Varwig, D. R. Yakovlev, D. Reuter, A. D. Wieck, and M. Bayer, Effect of pump-probe detuning on the Faraday rotation and ellipticity signals of mode-locked spins in (In,Ga)As/GaAs quantum dots, Phys. Rev. B **82**, 155325 (2010).

[41] S. G. Carter, A. Shabaev, S. E. Economou, T. A. Kennedy, A. S. Bracker, and T. L. Reinecke, Directing Nuclear Spin Flips in InAs Quantum Dots Using Detuned Optical Pulse Trains, Phys. Rev. Lett. **102**, 167403 (2009).

[42] V. L. Korenev, Multiple stable states of a periodically driven electron spin in a quantum dot using circularly polarized light, Phys. Rev. B **83**, 235429 (2011).

[43] M. M. Glazov, I. A. Yugova, and A. L. Efros, Electron spin synchronization induced by optical nuclear magnetic resonance feedback, Phys. Rev. B **85**, 041303(R) (2012).

[44] S. A. Crooker, J. Brandt, C. Sandfort, A. Greilich, D. R. Yakovlev, D. Reuter, A. D. Wieck, and M. Bayer, Spin Noise of Electrons and Holes in Self-Assembled Quantum Dots, Phys. Rev. Lett. **104**, 036601 (2010).

[45] V. S. Zapasskii, Spin-noise spectroscopy: From proof of principle to applications, Adv. Opt. Photon. **5**, 131 (2013).

[46] J. Hübner, F. Berski, R. Dahbashi, and M. Oestreich, The rise of spin noise spectroscopy in semiconductors: From acoustic to GHz frequencies, Phys. Status Solidi B **251**, 1824 (2014).

[47] Ph. Glasenapp, D. S. Smirnov, A. Greilich, J. Hackmann, M. M. Glazov, F. B. Anders, and M. Bayer, Spin noise of electrons and holes in (In,Ga)As quantum dots: Experiment and theory, Phys. Rev. B **93**, 205429 (2016).

[48] Z. G. Yu, Spin Hall Effect in Disordered Organic Solids, Phys. Rev. Lett. **115**, 026601 (2015).

[49] T. Holstein, Hall Effect in Impurity Conduction, Phys. Rev. **124**, 1329 (1961).

[50] T. V. Shahbazyan and M. E. Raikh, Low-Field Anomaly in 2D Hopping Magnetoresistance Caused by Spin-Orbit Term in the Energy Spectrum, Phys. Rev. Lett. **73**, 1408 (1994).

[51] S. H. Chun, M. B. Salamon, Y. Lyanda-Geller, P. M. Goldbart, and P. D. Han, Magnetotransport in Manganites and the Role of Quantal Phases: Theory and Experiment, Phys. Rev. Lett. **84**, 757 (2000).

[52] O. Entin-Wohlman, A. Aharony, Y. M. Galperin, V. I. Kozub, and V. Vinokur, Orbital ac Spin-Hall Effect in the Hopping Regime, Phys. Rev. Lett. **95**, 086603 (2005).

[53] B. I. Shklovskii and A. L. Efros, *Electronic Properties of Doped Semiconductors* (Springer, Berlin, 1984).

[54] Yu. A. Firsov, *Polarons* (Nauka, Moscow, 1975).

[55] H. Böttger and V. V. Bryksin, Hopping conductivity in ordered and disordered solids (I), Phys. Status Solidi B **78**, 9 (1976).

[56] B. I. Shklovskii and B. Z. Spivak, in *Scattering and Interference Effects in Variable Range Hopping Conduction in Hopping Transport in Solids*, edited by B. M. Pollak and B. Shklovskii (Elsevier, Amsterdam, 1991).

[57] A. V. Shumilin and V. I. Kozub, Interference mechanism of magnetoresistance in variable-range hopping conduction: The effect of paramagnetic electron spins and continuous spectrum of scatterer energies, Phys. Rev. B **85**, 115203 (2012).

[58] Y. M. Galperin, E. P. German, and V. G. Karpov, Hall effect under hopping conduction conditions, Zh. Eksp. Teor. Fiz. **99**, 343 (1991) [Sov. Phys. JETP **72**, 193 (1991)].

[59] D. Xiao, M.-C. Chang, and Q. Niu, Berry phase effects on electronic properties, Rev. Mod. Phys. **82**, 1959 (2010).

[60] M. V. Berry, Quantal phase factors accompanying adiabatic changes, Proc. R. Soc. London A **392**, 45 (1984).

[61] Ka Shen, G. Vignale, and R. Raimondi, Microscopic Theory of the Inverse Edelstein Effect, Phys. Rev. Lett. **112**, 096601 (2014).

[62] S. Mertens and C. Moore, Continuum percolation thresholds in two dimensions, Phys. Rev. E **86**, 061109 (2012).

[63] O. V. Dimitrova, Spin-hall conductivity in a two-dimensional Rashba electron gas, Phys. Rev. B **71**, 245327 (2005).

[64] B. I. Shklovskii, Dyakonov-perel spin relaxation near the metal-insulator transition and in hopping transport, Phys. Rev. B **73**, 193201 (2006).

[65] I. S. Lyubinskiy, Spin relaxation in the impurity band of a semiconductor in the external magnetic field, JETP Lett. **88**, 814 (2008).

[66] A. V. Shumilin and V. V. Kabanov, Kinetic equations for hopping transport and spin relaxation in a random magnetic field, Phys. Rev. B **92**, 014206 (2015).

[67] R. C. Roundy and M. E. Raikh, Spin relaxation of a diffusively moving carrier in a random hyperfine field, Phys. Rev. B **90**, 201203 (2014).

[68] V. V. Mkhitaryan and V. V. Dobrovitski, Hyperfine-induced spin relaxation of a diffusively moving carrier in low dimensions: Implications for spin transport in organic semiconductors, Phys. Rev. B **92**, 054204 (2015).

[69] L. M. Woods, T. L. Reinecke, and Y. Lyanda-Geller, Spin relaxation in quantum dots, Phys. Rev. B **66**, 161318 (2002).